Light Induced Forces on Dielectric Nanospheres

MAT-3900 Master's thesis in applied mathematics

Trine Lundamo

February 13, 2008

Faculty of Science
Department of Mathematics and Statistics
University of Tromsø

Light Induced Forces on Dielectric Nanospheres

MAT-3900 Master's thesis in applied mathematics

Trine Lundamo

February 13, 2008

Faculty of Science
Department of Mathematics and Statistics
University of Tromsø

I Abstract

Waves that are reflected and refracted by material bodies also transfer momentum to these bodies. This means that the wave field induces a force on the bodies, and multiple reflections between bodies induce forces between them.

Light is an electromagnetic wave phenomenon, and the waves carry energy and momentum. Hence, any object that is scattering and refracting light is also acted upon by a light induced force. This force is a tiny force and is usually ignored, but if the objects are small enough the force induced by the light field would dominate all other forces. Due to this it is possible to manipulate small objects using light from a laser.

This thesis is based on an experiment on optical binding of two dielectric spheres, where the spheres were small enough to make the force induced by the light field the dominating force. In the experiment bistability and hysteresis in the equilibrium separations of the optically bound dielectric spheres were observed in one dimension. In this thesis the experiment will be modeled with a simplified setup, and the goal is to see if it is possible to find bistability in two dimensions also. Numerical approximations are used to calculate the wave field, and from this the force on the objects can be found.

II Acknowledgment

This thesis concludes my education in applied mathematics at the University of Tromsø. I would like to express my gratitude to all the people that have supported me during this time.

First of all I would like to thank my supervisor associate professor Per K. Jakobsen for being an excellent teacher, and also for his encouragement and support.

Thanks to my fellow students for good conversations and company.

Thanks to my family for being there for me, and believing in me.

Last but not least I would like to thank my boyfriend Alexander Os. Thank you for your patience with me in the hardest periods.

Tromsø February 13, 2008

Trine Lundamo
sign.

Contents

List of Tables

List of Figures

III Nomenclature

α : constant, interval variable

γ : Euler or Euler-Mascheroni constant $\gamma = 0.5772156649$

Δx : grid size

$\delta(\mathbf{x})$: two dimensional Dirac delta function

δ_{ij} : Kronecker's delta

ε : electrical permittivity of material

ε_0 : permittivity of free space, $\varepsilon = 8.85 \times 10^{-12}\, C^2/Nm$

ϵ : variable

ζ : space variable in $\mathbb{R}^2$

θ, ϑ, Θ : polar coordinates

λ : wave length

μ : magnetic permeability of material, micro

μ_0 : permeability of free space, $4\pi \times 10^{-7}\, N/A^2$

ρ : polar coordinate

τ : period, $\tau = 2\pi \backslash \omega$

φ : wave function

φ_i : incoming wave

φ_r : reflected wave

φ_t : transmitted wave

ψ : scalar function

Ω, Ω_j : domain

Ω^c : domain, complement of Ω

ω : angular frequency

A_m : variable for φ_i

A_x, A_y, A_z : complex amplitudes

a : cylinder radius

$\mathbf{B}$: magnetic induction (field)

B_0 : norm of magnetic induction

$\mathbf{b}$: vector

b : confocal parameter

c : speed of light, $c = 3.00 \times 10^8\, m/s$

$\mathbf{D}$: electric displacement (field), $\mathbf{D} = \varepsilon \mathbf{E}$ in linear material

d : distance between cylinders/spheres

dx : infinitesimal

$\partial\Omega$: boundary of Ω

$\frac{dv}{dx}$, $v'(x)$: derivative of v(x)

$\frac{d^2v}{dx^2}$, $v''(x)$: two times derivative of v(x)

$\partial_x v$, v_x, $\frac{\partial v}{\partial x}$: partial derivative of v

$\frac{\partial v}{\partial \mathbf{n}}$, $\nabla v \cdot \mathbf{n}$, $\partial_{\mathbf{n}} v$: directional derivative of v in the direction of $\mathbf{n}$

$\mathbf{E}$: electric field

E_0 : norm of electric amplitude

e_x, e_y, e_z : unit vectors in the cartesian coordinate system

F : Force

$\mathbf{f}$: force vector

f : scalar function

G_j : Green's function for domain j

$\mathbf{H}$: magnetic field, $\mathbf{H} = \frac{1}{\mu_0}\mathbf{B}$

$H_m^{(1)}$, $H_m^{(2)}$: Hankel function of the first and second kind

$\mathbf{I}$: identity matrix

I : intensity of Gaussian beam

i : imaginary unit, index

$\mathbf{J}_j$: Laser source

J_m : Bessel function of the first kind

j : index, function

K_m : modified Bessel function of the second kind

k : propagation (or wave) vector

k : wave number, $k = \frac{\omega}{c}$, Boltzmann's constant

L : length scale

l : index

M : block matrix

m : index, meter, milli

N : number of grid points, newton

n : normal vector

n, n_j : refraction index

P : total energy flux, power

p : variable

Q_m : constant for φ_t

$\mathbf{q} = (x', y')$: space coordinate in $\mathbb{R}^2$

q : variable

$\mathbf{R} = (x, y)$: space coordinate in $\mathbb{R}^2$

R : polar coordinate

R_j : variable, $R_j = kn_j r$

R_m : constant for φ_r

r, r : polar coordinate

S : Poynting's vector

S_m : constant for φ_r

T : Maxwell's stress tensor

T : time

T_m : constant for φ_t

$\mathbf{t}$: tangential vector

t : time variable

V : volume, potential, spheres

$\mathbf{v}$: vector

W : beam radius for Gaussian beam, watt

W_0 : beam waist for Gaussian beam

$\mathbf{X}$: vector

x, y, z : space coordinates in $\mathbb{R}$

$\mathbf{x} = (x, y)$, $\mathbf{x} = (x, y, z)$: space coordinate in $\mathbb{R}^d$, $d = 2, 3$

Y_m : Bessel function of the second kind

$\hat{z}$: fourier transform of z

$|z|$: absolute value of z

$||\mathbf{z}||$: norm of $\mathbf{z}$

z^T : transpose of z

$< z >$: time average of z

z^* : complex conjugate of $z \in \mathbb{C}$

$\tilde{z}$: dimensionless variable

$\mathcal{L}$: differential operator, $\mathcal{L} = \nabla^2 + k^2 n_j^2$

$\mathcal{C}, \mathcal{S}$: contours, surface

$\nabla^2 v$: Laplacian operator applied to v

$\nabla \mathbf{v}$: gradient of v

$\nabla \times \mathbf{v}$: curl of $\mathbf{v}$

$\nabla \cdot \mathbf{v}$: divergence of $\mathbf{v}$

$\mathbf{k} \cdot \mathbf{x}$: inner product of the vectors $\mathbf{k}$ and $\mathbf{x}$

$\sum$: summation

1 Introduction

Waves that are reflected and refracted by material bodies also transfer momentum to these bodies. This means that the wave field induces a force on the bodies, and multiple reflections between bodies induce forces between them.

Light is an electromagnetic wave phenomenon, and is described by the same theoretical principles that determine all forms of electromagnetic radiation [1]. These waves carry energy and momentum, which can be imparted during interaction with matter. Hence, any object that is scattering and refracting light, is also acted upon by a light induced force. However, this force is tiny for ordinary sized objects and is therefore usually ignored. On the other hand, the force induced by the light field would dominate all other forces if the objects were small enough. Due to this, it is possible to manipulate small objects using light from a laser. The first known experimental demonstration of this phenomenon dates from 1971 [2]. Ever since, the technique has been extended and greatly refined, and today plays a major role in the ongoing nanotechnology revolution, where the goal is to engineer structures on the scale of molecules.

The interaction between objects and light waves can be treated in different ways, depending on the ratio between the size of the object and the wavelength of the light. If the wavelength is much smaller than the object, the interaction can be treated analytically using the geometric optics approximation [3]. In the opposite case, where the wavelength is much larger than the size of the object, the dipole approximation would be used [4]. And last, for the case where the wavelength of the wave field is of the order of the size of the bodies, only very symmetrical situations can be given an analytic treatment. A combination of analytical and numerical approximations, or a purely numerical approach, would be necessary for most realistic situations. If the goal is to calculate the refracted and scattered wave field in space, domain methods are most commonly used. They include finite difference, finite element and spectral (fourier) methods.

According to the Minkowski form of the Energy-Momentum tensor for a material body [5], when light interacts with homogeneous dielectric bodies, the force on the bodies can be calculated from the light field on the surface of each body. In this situation the boundary integral method would be used for calculating the force [6, 7, 8]. Boundary integral formulations eliminate two of the problems for the domain methods. The bounding surfaces are usually compact so the method is formulated on a finite domain, and sharp jumps in the refraction indices at the surfaces are not a problem since the method uses only the field values on the boundary. In addition, the method reduces the dimension of the problem by one, which leads to a large reduction in the size of the computational problem.

This thesis is based on an experiment on optical binding of two dielectric

spheres performed by Metzger et al. [9]. In the experiment they considered the case of small particles modeled as dielectric spheres, interacting through the optical field generated by counterpropagating laser beams from nearby optical waveguides. They observed bistability and hysteresis in the equilibrium separations of the optically bound dielectric spheres in one dimension.

The numerical calculation in the paper by Metzger et al. [9], was performed using the paraxial wave equation. In this method one assumes that the wave vectors for the wave field only have a small transverse component, and that there is no backscattering. In their experiment the spheres were so large that both assumptions are highly questionable. In this thesis the aim is to calculate forces and light scattering by using the boundary integral method. This method is not subject to any limitations on wave vectors or backscattering.

The setup for the problem in this thesis will have some simplifications compared to the setup for the experiment. First of all, the problem will be reduced from three dimensions involving spheres, to two dimensions involving infinitely long cylinders. In addition, only one laser beam will be used instead of two in the experiment. The two beams were incoherent, so this is in fact equivalent in a certain sense. In Chapter 3 this reduction in the number of sources will be discussed in more detail.

In the next chapter a brief resumé of the experiment performed by Metzger et al. [9] will be given, and the third chapter explains the setup for the problem handled in this paper. The fourth chapter will describe the exact solution for one cylinder, and an approximate solution to the same problem will be derived in chapter five. Then chapter six and seven will model the experiment by introducing a second cylinder and a Gaussian beam modeling the laser. A scaling of the problem is performed in chapter eight, while in chapter nine the force on the particles will be calculated. In the end a conclusion will be given.

2 Optical Binding of Two Dielectric Spheres

As mentioned in the introduction, an experiment on optical binding of two dielectric spheres is the background for this paper. In the experiment they found that by using a dual-beam fiber optic trap, bistability and hysteresis in the equilibrium separations of a pair of optically bound dielectric spheres were observed in one dimension [9]. The observations were in agreement with a coupled system model, in which the dielectric spheres modified the field propagation. Also, the field self-consistently determined the optical forces on the spheres. The results from the experiment revealed up to then unsuspected complexity in the coupled light-sphere system. A resumé from the experiment, based on the article by Metzger et al. [9], will be given in the following.

2.1 Experimental setup

The one-dimensional optically bound system, consisted of an isolated pair of colloidal microspheres that were held in a dual-beam, optical-fiber trap. The setup for the whole system with spheres and lasers can be seen in Figure 1. The equilibria positions were explored thoroughly, and revealed up to then unsuspected complexity. One was the observation of bistability in the sphere separations depending on the difference in the refraction indices for the spheres and the host medium. In addition, hysteresis in the trap equilibrium separations when varying the fiber separation was observed.

The setup for the model comprised two laser fields of wavelength λ, counterpropagating along the z-axis, which interacted with a pair of transparent dielectric spheres. The spheres were immersed in a host medium with a refraction index lower than for the spheres. The counterpropagating fields originated from two fibers placed on each side of the two spheres, making a symmetrical system along the horizontal line, as seen in Figure 1. The output field was modeled as identical collimated Gaussian beams with specified spot size and power. The spatial evolution of the counterpropagating fields due to the spheres were modeled by the paraxial wave theory which is described in Ref. [10].

The counterpropagating fields for a given configuration of the two spheres, were in turn used to calculate the optical force acting along the horizontal axis on each sphere. The two counterpropagating beams were assumed to be mutually incoherent, hence any interference between them were neglected.

The coupled equations for the counterpropagating fields and the optical forces acting on the spheres, were solved numerically to find the equilibrium sphere spacing where the net force acting on each sphere was zero. The equilibrium spacing was found to be stable when the derivative of the total force, with respect to the sphere separations, was less than zero at the zero crossing. It was assumed in the model that the spheres would remain well

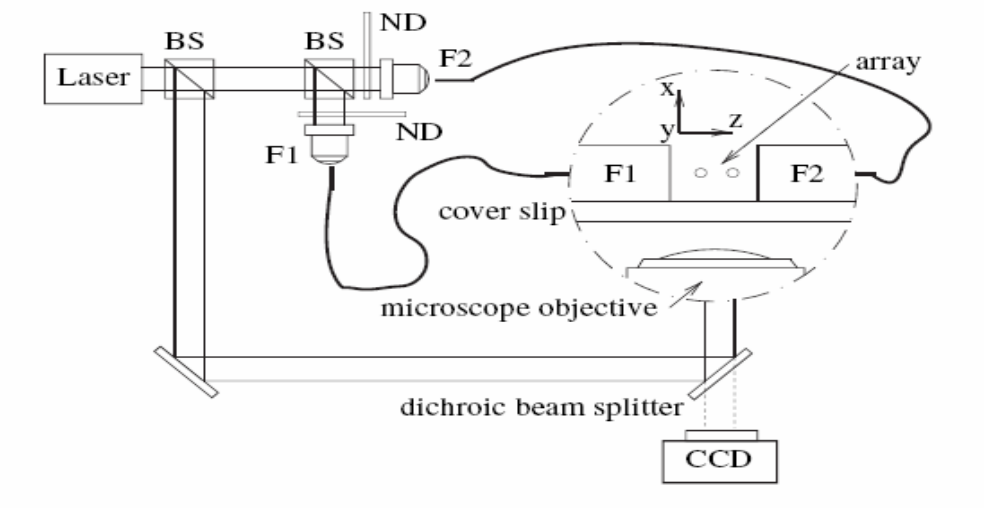

Figure 1: Setup from the experiment. Laser and first beam splitter (BS) for optical tweezers coupled through a dichroic beam splitter. Second beam splitter for fiber coupling (F1 and F2) with neutral density filters (ND). The magnified inset shows both fibers mounted on the cover slip. The array is formed between the two fiber-faces and observed from underneath the setup through the microscope objective and the dichroic beam splitter with a CCD camera [9].

confined in the plane transverse to the horizontal axis by virtue of the optical forces provided by the transverse structure of the counterpropagating fields. Hence the sphere motion was confined to the horizontal axis.

The bistability result from the experiment can be seen in Figure 2. It shows the numerically predicted sphere equilibrium separations together with the experimental results. It can be seen from the figure that for $\Delta n <= 0.076$ only one equilibrium is present, while for $\Delta n > 0.076$ three equilibrium states appear. The middle solution was found to be unstable though. So the coupled light-matter system exhibits regions of stability, namely two stable solutions for a given set of parameters.

Now, the goal of this paper is to model the experiment. But there will be some simplifications compared to the setup from the experiment. These simplifications will be covered in the next chapter.

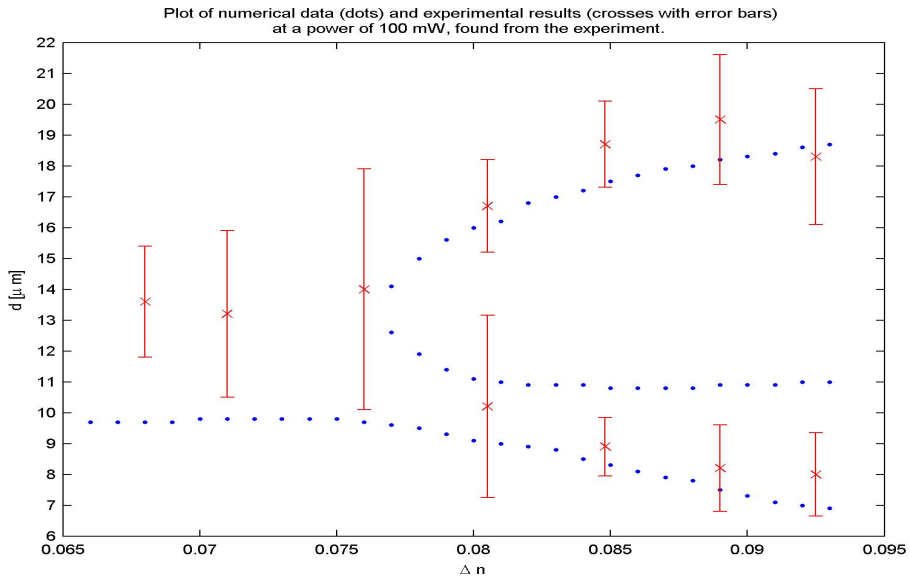

Figure 2: Result from the experiment with numerical data (dots) and experimental results (crosses with error bars). The crosses indicate the over all mean sphere separation d, and the error bars represent the distribution of the mean values with their standard deviations. The test was performed by changing the refraction index for the host medium (deionized water and sucrose solutions), and the spacing d between the spheres [9].

3 Setup for the Problem

Numerical calculations will be performed to try to find results that are similar to those found in the experiment summarized in the previous chapter. The numerical approximations will be performed on a simplified system compared to the setup that was used in the experiment, and these simplifications might lead to different results. The conclusion in the end of the paper will show if this is the case, or if the results are similar to those found in the experiment despite the simplifications. The simplifications described in the rest of this chapter are introduced in order to make the problem more tractable from a numerical point of view.

3.1 Problem in two dimensions

Instead of spheres that were used in the experiment, infinitely long cylinders will be used for the problem covered in this paper. Hence the setup will be in two instead of three dimensions, which will reduce the size of the computational problem quite a lot. The question is how different the waves will act in two compared to three dimensions.

3.2 One laser beam

In the experiment two laser beams were used, one placed on each side of the two spheres, making a symmetrical system about the y-axis. The distance between the two spheres was varied, and the situation of interest was when the total force on each sphere was zero. In this paper, only one laser beam will be used, and it will be placed on the left side of the two cylinders. This simplification can be introduced because the beams used in the experiment were incoherent. The reduction in the number of sources is supported in the following.

Let $\mathbf{J}_1$ and $\mathbf{J}_2$ be two laser sources and let $\mathbf{E}_1$, $\mathbf{B}_1$ and $\mathbf{E}_2$, $\mathbf{B}_2$ be the electromagnetic fields generated by each source separately. Due to the linearity of Maxwell's equations in a dielectricum [11], the fields generated by the combined sources are

$$\mathbf{E} = \mathbf{E}_1 + \mathbf{E}_2 \quad \text{and} \quad \mathbf{B} = \mathbf{B}_1 + \mathbf{B}_2 \tag{3.1}$$

The average force on an object V is given as [12]

$$\mathbf{f}_{av} = \int_{\partial V} < \mathbf{T} > \cdot \mathbf{n}\, dS \tag{3.2}$$

Where $< >$ is time average, and $\mathbf{T}$ is the Maxwell stress tensor given as [11]

$$\mathbf{T} = \varepsilon \mathbf{E}\mathbf{E} + \frac{1}{\mu_0}\mathbf{B}\mathbf{B} - \frac{1}{2}\mathbf{I}\left(\varepsilon \mathbf{E}\cdot\mathbf{E} + \frac{1}{\mu_0}\mathbf{B}\cdot\mathbf{B}\right) \tag{3.3}$$

The stress tensor for the field generated by the combined sources is given as

$$\begin{aligned} \mathbf{T} &= \varepsilon(\mathbf{E}_1+\mathbf{E}_2)(\mathbf{E}_1+\mathbf{E}_2) + \frac{1}{\mu_0}(\mathbf{B}_1+\mathbf{B}_2)(\mathbf{B}_1+\mathbf{B}_2) \\ &\quad - \frac{1}{2}\mathbf{I}\Big(\varepsilon(\mathbf{E}_1+\mathbf{E}_2)\cdot(\mathbf{E}_1+\mathbf{E}_2) + \frac{1}{\mu_0}(\mathbf{B}_1+\mathbf{B}_2)\cdot(\mathbf{B}_1+\mathbf{B}_2)\Big) \end{aligned} \tag{3.4}$$

And the time averaged stress tensor can then be written as

$$\begin{aligned} < \mathbf{T} > &= < \mathbf{T}_1 > + < \mathbf{T}_2 > + \varepsilon < \mathbf{E}_1\mathbf{E}_2 > + \varepsilon < \mathbf{E}_2\mathbf{E}_1 > + \frac{1}{\mu_0} < \mathbf{B}_1\mathbf{B}_2 > \\ &\quad + \frac{1}{\mu_0} < \mathbf{B}_2\mathbf{B}_1 > - \frac{1}{2}\mathbf{I}\Big(\varepsilon < \mathbf{E}_1\cdot\mathbf{E}_2 > + \varepsilon < \mathbf{E}_2\cdot\mathbf{E}_1 > \\ &\quad + \frac{1}{\mu_0} < \mathbf{B}_1\cdot\mathbf{B}_2 > + \frac{1}{\mu_0} < \mathbf{B}_1\cdot\mathbf{B}_2 >\Big) \end{aligned} \tag{3.5}$$

Due to the incoherence of the sources $\mathbf{J}_1$ and $\mathbf{J}_2$,

$$< \mathbf{E}_1\mathbf{E}_2 > = < \mathbf{E}_2\mathbf{E}_1 > = < \mathbf{B}_1\mathbf{B}_2 > = < \mathbf{B}_2\mathbf{B}_1 > = 0 \tag{3.6}$$

And the time average over the dot products are also zero. Hence, the time averaged stress tensor is written as

$$< \mathbf{T} > = < \mathbf{T}_1 > + < \mathbf{T}_2 > \tag{3.7}$$

From this, the average force is found to be

$$\mathbf{f}_{av} = \int_{\partial V} (< \mathbf{T}_1 > + < \mathbf{T}_2 >) \cdot \mathbf{n} \, dS = \mathbf{f}_1 + \mathbf{f}_2 \tag{3.8}$$

The forces are therefore additive for incoherent sources. Now, let V_1 and V_2 be two spheres placed symmetrical with respect to the midplane and the sources $\mathbf{J}_1$ and $\mathbf{J}_2$, see Figure 3.

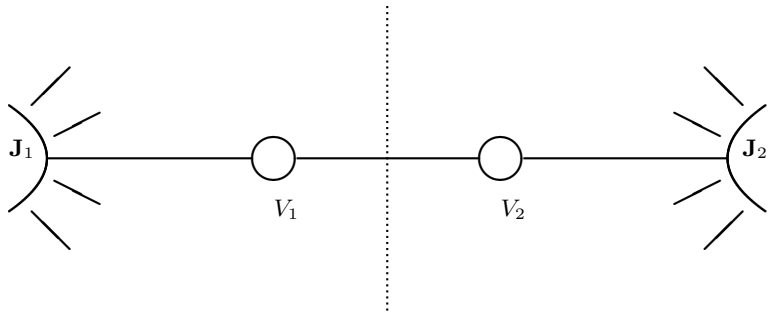

Figure 3: Two spheres, V_1 and V_2, and two sources, $\mathbf{J}_1$ and $\mathbf{J}_2$, placed symmetrical about the y-axis.

Let $\mathbf{f}_1$ and $\mathbf{f}_2$ be the forces on V_1 and V_2 from the combined sources, and let $\mathbf{f}_{ij}$ be the force on object i induced by source j. This gives

$$\mathbf{f}_1 = \mathbf{f}_{11} + \mathbf{f}_{12} \tag{3.9}$$

$$\mathbf{f}_2 = \mathbf{f}_{21} + \mathbf{f}_{22} \tag{3.10}$$

The symmetry of the setup gives

$$\mathbf{f}_{11} = -\mathbf{f}_{22}, \text{ and } \mathbf{f}_{21} = -\mathbf{f}_{12} \tag{3.11}$$

The force $\mathbf{f}$, which determines the relative acceleration of the spheres, is given as $\mathbf{f} = \mathbf{f}_2 - \mathbf{f}_1$. This, together with the relations found in the equation above, gives the following expression for the force:

$$\mathbf{f} = \mathbf{f}_{21} - \mathbf{f}_{11} - \mathbf{f}_{11} + \mathbf{f}_{21} = 2\,(\mathbf{f}_{21} - \mathbf{f}_{11}) \tag{3.12}$$

Thus, the force $\mathbf{f}$ is zero if and only if $\mathbf{f}_{21} - \mathbf{f}_{11} = 0$, which only involves forces from source one. This shows that it is possible to use only one source in this paper.

The actual motion of the scattering objects will be different for one and two sources. In the experiment the situation of interest was when the total force on each sphere was zero, hence the spheres were standing still. For the simplified problem with only one laser beam, the corresponding situation will be when the force on cylinder one, equals the force on cylinder two. Then the two cylinders will move with a constant distance between them, which will be analogous to the situation in the experiment where the two spheres were standing still.

3.3 One cylinder and a planar wave

In the beginning of the paper a couple of extra simplifications will be used. The numerical procedures will first include only one cylinder in the system, and the incident wave will have the form of a plane wave. For this situation the exact solution can be calculated. An approximation to the exact solution will then be derived and compared to the exact solution, to see if they resemble each other. If the approximative solution is good, it will be developed further to include two cylinders and a Gaussian beam modeling the laser.

Hence the problem in two dimensions is the following: An infinitely long cylinder is placed along the z-axis. A light-source placed far away from the cylinder sends out waves that have the form of plane waves when they reach the cylinder. Figure 4 gives a sketch of the problem. A plane wave will hit the cylinder, Ω, and will be scattered depending on the refraction indices of the cylinder and the host medium.

Figure 4: A source is sending out waves from far away. When these waves are getting close to the cylinder, they can be seen as plane waves (the parallel lines in the figure). When a wave hit the cylinder, it will be scattered based on the refraction indices of the cylinder and the host medium. The wavelength and the diameter of the cylinder, are of the same order of magnitude.

In the next chapter the exact solution for the wave field arising from this setup will be calculated.

4 Exact Solution for One Cylinder

The goal for this chapter is to find the exact solution of the wave function for the scattering in the two-dimensional problem given in the previous chapter. The solution will be calculated both on the boundary of the cylinder, and for a given domain. To solve the problem, the starting point will be the governing equations of electromagnetics, namely the Maxwell equations.

4.1 Maxwell's equations

The Maxwell equations in a material with no free currents and charges are given as [11]:

$$\nabla \times \mathbf{E} + \frac{\partial \mathbf{B}}{\partial t} = 0 \tag{4.1}$$

$$\nabla \times \mathbf{H} - \frac{\partial \mathbf{D}}{\partial t} = 0 \tag{4.2}$$

$$\nabla \cdot \mathbf{B} = 0 \tag{4.3}$$

$$\nabla \cdot \mathbf{D} = 0 \tag{4.4}$$

The basic electromagnetic fields are the electric field $\mathbf{E}$ and the magnetic induction field $\mathbf{B}$. In addition there are the magnetic field $\mathbf{H}$ and the electric displacement field $\mathbf{D}$. The relations between the magnetic induction field $\mathbf{B}$ and the magnetic field $\mathbf{H}$, and between the electric field $\mathbf{E}$ and the electric displacement field $\mathbf{D}$, are given as

$$\mathbf{D} = \mathbf{D}[\mathbf{E}, \mathbf{B}] \tag{4.5}$$

$$\mathbf{H} = \mathbf{H}[\mathbf{E}, \mathbf{B}], \tag{4.6}$$

called the constitutive relations, meaning they describe the medium [13].

Assuming the field strengths are so small that the regime is linear, and the medium is nonmagnetic and isotropic, $\mathbf{E}(\mathbf{x}, \omega)$ and $\mathbf{D}(\mathbf{x}, \omega)$ are related by a scalar dielectric constant $\varepsilon(\mathbf{x}, \omega)$, also known as the electric permittivity of the material. The variables are the space coordinate, $\mathbf{x}$, and the frequency, ω. By choosing an appropriate value for the dielectric constant in the frequency range of the source, which is a continuous laser operating at a single frequency, the frequency dependence of $\varepsilon(\mathbf{x}, \omega)$ can be ignored. The two other fields, $\mathbf{B}(\mathbf{x}, \omega)$ and $\mathbf{H}(\mathbf{x}, \omega)$, are related by $\mu(\mathbf{x}, \omega)$, the magnetic permeability of the material. Since the material is nonmagnetic, $\mu(\mathbf{x}, \omega) = \mu_0$, where $\mu_0 = 4\pi \times 10^{-7} N/A^2$ is the permeability of free space. Taking all the

given information into account, the constitutive equations can be given as [11]:

$$\mathbf{D}(\mathbf{x}) = \varepsilon(\mathbf{x})\mathbf{E}(\mathbf{x}) \tag{4.7}$$

$$\mathbf{H}(\mathbf{x}) = \frac{1}{\mu_0}\mathbf{B}(\mathbf{x}) \tag{4.8}$$

The source sending out light waves is assumed to be monochromatic, meaning that the electromagnetic radiation is of a single wavelength. The equation for the source-field is given as:

$$\mathbf{J}(\mathbf{x},t) = \frac{1}{2}\left\{\mathbf{J}(\mathbf{x})e^{-i\omega t} + \mathbf{J}^*(\mathbf{x})e^{i\omega t}\right\} \tag{4.9}$$

A good laser operating in continuous mode approximates such a source very well.

From the form of the source-field, the electric and the magnetic fields are given as

$$\mathbf{E}(\mathbf{x},t) = \frac{1}{2}\left\{\mathbf{E}(\mathbf{x})e^{-i\omega t} + \mathbf{E}^*(\mathbf{x})e^{i\omega t}\right\} \tag{4.10}$$

$$\mathbf{H}(\mathbf{x},t) = \frac{1}{2}\left\{\mathbf{H}(\mathbf{x})e^{-i\omega t} + \mathbf{H}^*(\mathbf{x})e^{i\omega t}\right\} \tag{4.11}$$

Now, using what was found in Equations 4.7-4.11, Maxwell's equations simplifies to

$$\nabla \times \mathbf{E} - i\omega\mu_0\mathbf{H} = 0 \tag{4.12}$$

$$\nabla \times \mathbf{H} + i\omega\varepsilon\mathbf{E} = 0 \tag{4.13}$$

$$\nabla \cdot \varepsilon\mathbf{E} = 0 \tag{4.14}$$

$$\nabla \cdot \mathbf{H} = 0 \tag{4.15}$$

These stationary Maxwell equations will be used in the next section to derive the Helmholtz equation.

4.2 Helmholtz's equation

The well-known Helmholtz equation is often found in the study of physical problems involving wave phenomena. The equation will be derived from Maxwell's equations. The first step is to introduce the standard definition for the refraction index of a non-magnetic material, given as [11]

$$n(\mathbf{x},\omega) = \sqrt{\frac{\varepsilon(\mathbf{x},\omega)}{\varepsilon_0}} \tag{4.16}$$

Here ε_0 is the permittivity of free space, which can be found from $c^{-2} = \varepsilon_0\mu_0$, where c is the speed of light in vacuum, and the value of μ_0 was given in the

previous section. So for a given frequency domain the dielectric constant ε can be written as

$$\varepsilon(\mathbf{x}) = \varepsilon_0 n^2(\mathbf{x}) \tag{4.17}$$

The problem in this paper involves an infinitely long cylinder, with a given refraction index, placed along the z-axis. The refraction index is constant both in the domain inside the cylinder and in the domain outside the cylinder, that is the host medium. So the refraction index is stepwise constant, and is written n_j, where $j = 0, 1$ represents the outer domain and the cylinder respectively. Now, using the expression for ε that was found above, the divergence equation of the electric field, Equation 4.14, is rewritten as

$$\begin{aligned} \nabla \cdot (\varepsilon \mathbf{E}) &= 0 \\ \nabla \cdot (\varepsilon_0 n^2(\mathbf{x}) \mathbf{E}) &= 0 \\ \nabla \cdot (n^2(\mathbf{x}) \mathbf{E}) &= 0 \end{aligned} \tag{4.18}$$

The electric field is assumed to be parallel to the cylinder axis (z-axis), hence the electric field is transverse to the propagation direction of the wave, and only has a z-component. This means that the field can be written as $\mathbf{E}(x, y, z) = E(x, y)e_z$, and since the refraction index only depends on x and y, Equation 4.18 is automatically true and is rewritten as

$$\begin{aligned} \nabla \cdot \left(n^2(\mathbf{x})\, \mathbf{E}\right) &= \partial_z n^2(x, y) E(x, y) = 0 \\ \nabla \cdot \mathbf{E} &= 0 \end{aligned} \tag{4.19}$$

So the divergence of the electric field $\mathbf{E}$ is zero in homogeneous regions.

Calculating the curl of Maxwell's Equation 4.12, and using the relation for the curl of the $\mathbf{H}$-field found in Equation 4.13, gives the following

$$\begin{aligned} \nabla \times \nabla \times \mathbf{E} &= i\omega\mu_0 \left(\nabla \times \mathbf{H}\right) \\ &= i\omega\mu_0(-i\omega\varepsilon_0 n^2(\mathbf{x})\mathbf{E}) \\ &= \left(\frac{\omega n(\mathbf{x})}{c}\right)^2 \mathbf{E} \end{aligned} \tag{4.20}$$

Here $\mu_0\varepsilon_0$ has been replaced by c^{-2}. The same calculation can be written another way by applying the vector identity for $\nabla \times \nabla \times$, which gives [12]

$$\begin{aligned} \nabla \times \nabla \times \mathbf{E} &= \nabla \left(\nabla \cdot \mathbf{E}\right) - \nabla^2 \mathbf{E} \\ &= -\nabla^2 \mathbf{E} \end{aligned} \tag{4.21}$$

The fact that the divergence of $\mathbf{E}$ is zero has been used to get this result. Now, putting Equations 4.20 and 4.21 together gives

$$\begin{aligned} \left(\nabla^2 + \left(\frac{\omega n(\mathbf{x})}{c}\right)^2\right) \mathbf{E} &= 0 \\ \left(\nabla^2 + k^2 n^2(\mathbf{x})\right) \mathbf{E} &= 0 \end{aligned} \tag{4.22}$$

The wave number k comes from the relation: $k \stackrel{def}{=} \omega/c$, where ω is the angular frequency of the wave, and c is the speed of light as mentioned earlier. Equation 4.22 is known as Helmholtz's equation.

4.3 Bessel's equation

When looking for a solution to Helmholtz's equation in cylindrical (or spherical) coordinates, the Bessel equation often arises. So in this section Bessel's equation will be derived from Helmholtz equation.

As mentioned in Section 4.2, the electric field is transverse to the propagation direction of the waves. Hence, the electric field only has a z-component: $\mathbf{E} = (0, 0, E_z)$. Set $E_z = \varphi$, where φ is the wave function. The Helmholtz equation for the wave function then becomes

$$\nabla^2\varphi + k^2n^2(\mathbf{x})\varphi = 0 \tag{4.23}$$

The system is oriented so that a plane wave enters from the left, propagating in the x-direction, see Figure 4 on page 8. Using polar coordinates the Helmholtz equation for φ can be written as

$$\nabla^2\varphi(r,\theta) + k^2n^2(r,\theta)\varphi(r,\theta) = 0 \tag{4.24}$$

The cylinder is placed with its center in the origin, hence r is the distance from the origin, and θ is the angle for vector $\mathbf{r}$ with $\theta \in [0, 2\pi]$. Since $\varphi(r,\theta)$ is periodic in θ, the wave function can be written as the following sum:

$$\varphi(r,\theta) = \sum_m \varphi_m(r)e^{im\theta} \tag{4.25}$$

The unknown $\varphi_m(r)$ needs to be found to get an expression for the wave function.

Given a function $f(r,\theta)$, the Laplace operator ∇^2 in cylindrical coordinates gives

$$\nabla^2 f(r,\theta) = \frac{1}{r}\frac{\partial}{\partial r}\left(r\frac{\partial f}{\partial r}\right) + \frac{1}{r^2}\frac{\partial^2 f}{\partial\theta^2} \tag{4.26}$$

Replacing f with the wave function φ, that was found in Equation 4.25, gives

$$\begin{aligned}\nabla^2\Big(\sum_m \varphi_m(r)e^{im\theta}\Big) &= \frac{1}{r}\frac{\partial}{\partial r}\left(r\frac{\partial}{\partial r}\sum_m \varphi_m(r)e^{im\theta}\right) + \frac{1}{r^2}\frac{\partial^2}{\partial\theta^2}\sum_m \varphi_m(r)e^{im\theta} \\ &= \sum_m\left(\frac{1}{r}\varphi'_m(r)e^{im\theta} + \varphi''_m(r)e^{im\theta} - \frac{m^2}{r^2}\varphi_m(r)e^{im\theta}\right)\end{aligned} \tag{4.27}$$

From this, the polar form of the Helmholtz equation for the wave function can be written as

$$\sum_m\left[\varphi''_m(r)e^{im\theta} + \frac{1}{r}\varphi'_m(r)e^{im\theta} - \Big((\frac{m}{r})^2 - k^2n^2(r)\Big)\varphi_m(r)e^{im\theta}\right] = 0 \tag{4.28}$$

Each term in the sum is a coefficient of the exponential function $e^{im\theta}$, and these are linearly independent. Due to this, all the terms in the sum must be zero, so each m gives

$$\varphi_m''(r) + \frac{1}{r}\varphi_m'(r) + \Big(k^2 n^2(r) - (\frac{m}{r})^2\Big)\varphi_m(r) = 0 \tag{4.29}$$

This equation resembles the well-known Bessel equation given as [14]

$$x^2\frac{d^2y}{dx^2} + x\frac{dy}{dx} + (x^2 - \alpha^2)y = 0 \tag{4.30}$$

It can be seen that with a few operations, Equation 4.29 can be transformed into Bessel's equation when $n(r)$ is constant. Remember that $n(r)$ is a stepwise constant function written as n_j, where $j = 0, 1$ depending on the domain. First, the equation is multiplied by r^2 to get

$$r^2\varphi_m''(r) + r\varphi_m'(r) + (k^2 n_j^2 r^2 - m^2)\varphi_m(r) = 0 \tag{4.31}$$

Second, comparing this equation with Bessel's equation, shows that $k^2 n_j^2$ should equal one. To achieve this, r is replaced by a new variable $R_j = kn_j r$. The derivatives of $\varphi(R_j)$ then become

$$\varphi'(R_j) = \frac{d\varphi}{dR_j}\frac{dR_j}{dr} = kn_j\frac{d\varphi}{dR_j} \tag{4.32}$$

$$\varphi''(R_j) = k^2 n_j^2\frac{d^2\varphi}{dR_j^2} \tag{4.33}$$

Introducing R_j and the new derivatives for φ into Equation 4.31 gives

$$R_j^2\varphi_m''(R_j) + R_j\varphi_m'(R_j) + (R_j^2 - m^2)\varphi_m(R_j) = 0 \tag{4.34}$$

Hence, Bessel's equation for the wave function φ_m has been derived from Helmholtz's equation found in Equation 4.24. This means that the solution to Helmholtz's equation can be found as Bessel functions, known solutions to Bessel's equation. Before these functions are investigated any further, the different waves arising from the scattering of a plane wave will be discussed.

4.4 Incident, reflected and transmitted waves

The plane wave coming from the source far away from the cylinder is called the incident wave φ_i. The scattering of a plane wave hitting a cylinder with a different refraction index, results in a reflected wave, φ_r, and a transmitted wave, φ_t. The reflected wave together with the incident wave form the wave field outside the cylinder, while the transmitted wave forms the wave field inside the cylinder. From this the wave function $\varphi(r, \theta)$ can be written as

$$\varphi(r,\theta) = \varphi_i(r,\theta) + \varphi_r(r,\theta), \quad r \geq a \tag{4.35}$$

$$\varphi(r,\theta) = \varphi_t(r,\theta), \quad r < a \tag{4.36}$$

Where a is the radius of the cylinder.

The wave function φ represents the z-component of the electric field vector E_z, so the wave function is continuous across the interface between the cylinder and the host medium. Also the magnetic field, given as

$$\begin{aligned} \mathbf{H} &= \frac{1}{i\omega\mu_0}\nabla \times \mathbf{E} \\ &= \frac{1}{i\omega\mu_0}(\partial_y\varphi, -\partial_x\varphi, 0), \end{aligned} \tag{4.37}$$

is continuous across the interface since the material is nonmagnetic. When the magnetic field is continuous, so are $\partial_x\varphi$ and $\partial_y\varphi$, and hence the normal derivative of the wave function, $\partial_{\mathbf{n}}\varphi$, is also continuous across the interface. From this, the boundary conditions for Helmholtz's equation are given as

$$\varphi_t(a,\theta) = \varphi_i(a,\theta) + \varphi_r(a,\theta) \tag{4.38}$$

$$\partial_{\mathbf{n}}\varphi_t(a,\theta) = \partial_{\mathbf{n}}\varphi_i(a,\theta) + \partial_{\mathbf{n}}\varphi_r(a,\theta) \tag{4.39}$$

As mentioned in the end of the previous section, the basis functions for φ are the Bessel functions. The ones that will be used as a basis here, are the Bessel functions of the first and the second kind, $J_m(r)$ and $Y_m(r)$ respectively. Figure 5 shows the characteristics for these two Bessel functions of order zero and order one.

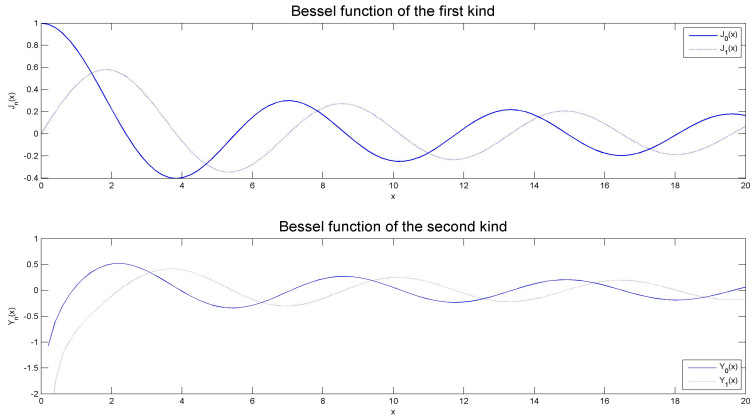

Figure 5: The Bessel function of the first kind is given in the upper plot and the Bessel function of the second kind is given in the lower plot. Both functions are given in the zeroth and first order. The Bessel function of the second kind is singular at $x = 0$.

The incident field $\varphi_i(r,\theta)$ is periodic in θ and can thus be written as $\varphi_i(r,\theta) = \sum_m A_m(r)e^{im\theta}$. The reflected and the transmitted waves are

written with the given basis of Bessel functions. Hence, the three wave types are given as

$$\varphi_i(r) = \sum_m A_m(r)e^{im\theta} \tag{4.40}$$

$$\varphi_t(r) = \sum_m (T_m J_m(r) + Q_m Y_m(r))e^{im\theta} \tag{4.41}$$

$$\varphi_r(r) = \sum_m (R_m J_m(r) + S_m Y_m(r))e^{im\theta} \tag{4.42}$$

Where T_m, Q_m, R_m and S_m are unknown constants that must be found. Having these three equations and the two boundary conditions given in Equations 4.38 and 4.39, one more condition is needed to make the system solvable, and that is the radiation condition. Arnold Sommerfeld defined the condition of radiation for a scalar field satisfying the Helmholtz equation as "the sources must be sources, not sinks, of energy. The energy which is radiated from the sources must scatter to infinity; no energy may be radiated from infinity into the [...] field." [15]. Hence, a wave that is reflected from the cylinder, should not return back again. To make sure this does not happen, the reflected wave function will be written in terms of the Hankel functions, $H_m^1(r)$ and $H_m^2(r)$. The Hankel functions, also known as Bessel functions of the third kind, are two linearly independent functions, which solve the Bessel equation. The functions are defined as $H_m^{(1,2)}(r) = J_m(r) \pm iY_m(r)$ [14]. Where i is the imaginary unit. The new equation for the reflected wave with Hankel functions as a basis is given as

$$\varphi_r(r) = \sum_m \Big(R_m H_m^{(1)}(r) + S_m H_m^{(2)}(r)\Big)e^{im\theta} \tag{4.43}$$

The Hankel functions for large arguments, $r >> 1$, are given as [16]

$$H_m^{(1)}(r) \approx \frac{1}{\sqrt{r}}e^{ir} \tag{4.44}$$

$$H_m^{(2)}(r) \approx \frac{1}{\sqrt{r}}e^{-ir} \tag{4.45}$$

The time variation $e^{-i\omega t}$ was previously assumed and suppressed, but taking this into account for the Hankel functions of large arguments, gives the following

$$\frac{1}{\sqrt{r}}e^{ir}e^{-i\omega t} = \frac{1}{\sqrt{r}}e^{i(r-\omega t)} \tag{4.46}$$

$$\frac{1}{\sqrt{r}}e^{-ir}e^{-i\omega t} = \frac{1}{\sqrt{r}}e^{-i(r+\omega t)} \tag{4.47}$$

It can be seen from these equations that the phase velocity for the Hankel function of the first kind is positive, which means the wave is going outwards.

The phase velocity for the Hankel function of the second kind is negative, hence it represents a wave going inwards. The reflected wave expression should not include a wave that goes inwards according to the *Sommerfeld's radiation condition* mentioned earlier in this section. Hence $H_m^{(2)}$ should not be a part of $\varphi_r(r,\theta)$, so S_m in Equation 4.43 must be zero.

A last simplification to the wave functions can be done to φ_t. The Bessel function of the second kind, Y_m, is singular for $r = 0$. Since the solution must be smooth, Q_m in Equation 4.41 is set to zero.

So now, introducing the new basis for φ_r, the simplification for φ_t, and then replacing r with $R_j = kn_j r$, which was found in the previous section, the incident, reflected and transmitted waves are found to be

$$\varphi_i(kn_0 r) = \sum_m A_m(kn_0 r)e^{im\theta} \tag{4.48}$$

$$\varphi_r(kn_0 r) = \sum_m R_m H_m^{(1)}(kn_0 r)e^{im\theta} \tag{4.49}$$

$$\varphi_t(kn_1 r) = \sum_m T_m J_m(kn_1 r)e^{im\theta} \tag{4.50}$$

Here n_0 is the refraction index of the host medium, and n_1 is the refraction index of the cylinder.

The next step will be to find the unknown coefficients of these equations, A_m, R_m and T_m.

4.4.1 The incident wave

The incident wave is, as mentioned earlier, a plane wave and can be written as $e^{i(\mathbf{k}\cdot\mathbf{x}-\omega t)}$ [12], where $\mathbf{k}$ is the propagation vector, and the amplitude of the wave has been set to one. The incident wave travels in the x-direction, hence the scalar number $\mathbf{k}\cdot\mathbf{x}$ simplifies to $kn(\mathbf{x})x$. Also, the time variation has been suppressed, so the plane wave is written as $e^{ikn(\mathbf{x})x} = e^{ikn_0 r\cos(\theta)}$, where $n(\mathbf{x})$ is set to n_0 since the incident wave is found in the host medium. This expression for a plane wave will now be used for calculating A_m in the expression for the incident wave φ_i, see Equation 4.48. The 2π-periodicity of $e^{ikn_0 r cos(\theta)}$ implies that

$$e^{ikn_0 r\cos(\theta)} = \sum_m A_m(kn_0 r)e^{im\theta}, \tag{4.51}$$

where

$$A_m(kn_0 r) = \frac{1}{2\pi}\int_0^{2\pi} e^{ikn_0 r\cos(\theta)}e^{-im\theta}\,d\theta \tag{4.52}$$

Using Euler's formula: $e^{ix} = \cos(x) + i\sin(x)$ [12], the expression for A_m can be split in two integrals which gives

$$A_m(kn_0r) = \frac{1}{2\pi}\int_0^{2\pi}(e^{ikn_0r\cos(\theta)}\cos(m\theta))\,d\theta - \frac{i}{2\pi}\int_0^{2\pi}(e^{ikn_0r\cos(\theta)}\sin(m\theta))\,d\theta \tag{4.53}$$

The latter integral is rewritten as follows

$$\begin{aligned}\int_0^{2\pi}(e^{ikn_0r\cos(\theta)}\sin(m\theta))\,d\theta &= \int_{-\pi}^{\pi}(e^{ikn_0r\cos(\theta+\pi)}\sin(m\theta+m\pi))\,d\theta \\ &= (-1)^m\int_{-\pi}^{\pi}(e^{-ikn_0r\cos(\theta)}\sin(m\theta))\,d\theta \\ &= 0 \end{aligned} \tag{4.54}$$

Here, the fundamental formulas for angle addition in trigonometry given as [17]

$$\cos(m\theta - m\pi) = \cos(m\theta)\cos(m\pi) + \sin(m\theta)\sin(m\pi) \tag{4.55}$$

$$\sin(m\theta - m\pi) = \sin(m\theta)\cos(m\pi) - \cos(m\theta)\sin(m\pi), \tag{4.56}$$

are used. The result in Equation 4.54 is zero because the integrand is odd. Now, by splitting up the first integral in Equation 4.53, the expression for A_m changes to

$$A_m(kn_0r) = \frac{1}{2\pi}\int_0^{\pi}(e^{ikn_0r\cos(\theta)}\cos(m\theta))\,d\theta + \frac{1}{2\pi}\int_{\pi}^{2\pi}(e^{ikn_0r\cos(\theta)}\cos(m\theta))\,d\theta \tag{4.57}$$

Then the integral limits are changed in order to get the same interval

$$A_m(kn_0r) = \frac{1}{2\pi}\int_0^{\pi}(e^{ikn_0r\cos(\theta)}\cos(m\theta))\,d\theta + \frac{1}{2\pi}\int_0^{\pi}(e^{ikn_0r(-\cos(\theta))}\cos(m\theta+m\pi))\,d\theta \tag{4.58}$$

The *cosine*-expression in the latter integral is replaced using the fundamental formula of angle addition given in Equation 4.55, so A_m is rewritten as

$$A_m(kn_0r) = \frac{1}{2\pi}\left(\int_0^{\pi}(e^{ikn_0r\cos(\theta)}\cos(m\theta))\,d\theta + (-1)^m\int_0^{\pi}(e^{-ikn_0r\cos(\theta)}\cos(m\theta))\,d\theta\right) \tag{4.59}$$

Bessel's first integral is found to be [18]

$$J_m(z) = \frac{i^{-m}}{\pi}\int_0^{\pi}(e^{iz\cos(\theta)}\cos(m\theta))d\theta \tag{4.60}$$

This integral is recognized in Equation 4.59, and simplifies the expression for A_m to

$$A_m(kn_0r) = \frac{i^m}{2}J_m(kn_0r) + (-1)^m\frac{i^m}{2}J_m(-kn_0r) \tag{4.61}$$

Given the following relation between two Bessel functions of the first kind [14],

$$J_m(-z) = (-1)^m J_m(z), \tag{4.62}$$

the final expression for $A_m(kn_0r)$ can be written as

$$A_m(kn_0r) = i^m J_m(kn_0r) \tag{4.63}$$

Hence the incident wave is found to be

$$\varphi_i = \sum_m i^m J_m(kn_0r)e^{im\theta} \tag{4.64}$$

4.4.2 Reflected and transmitted waves

Knowing A_m, it is possible to find the unknown values for the reflected and the transmitted waves found in Equations 4.49 and 4.50. Using the boundary condition given in Equation 4.38 on page 14 where $\varphi_i + \varphi_r = \varphi_t$ when $r = a$ gives

$$\begin{aligned}
&\sum_m A_m(kn_0r)e^{im\theta} + \sum_m R_m H_m^{(1)}(kn_0r)e^{im\theta} = \sum_m T_m J_m(kn_1r)e^{im\theta} \\
&\sum_m \left(i^m J(kn_0r) + R_m H_m^{(1)}(kn_0r) - T_m J_m(kn_1r)\right)e^{im\theta} = 0
\end{aligned} \tag{4.65}$$

In the latter equation, each term in the sum is a coefficient of the exponential function $e^{im\theta}$, and these are linearly independent. Hence, each term must be zero, which gives the following

$$i^m J_m(kn_0r) + R_m H_m^{(1)}(kn_0r) - T_m J_m(kn_1r) = 0 \tag{4.66}$$

Another equation is found by using the second boundary condition given in Equation 4.39 on page 14, where $\partial_{\mathbf{n}}\varphi_i + \partial_{\mathbf{n}}\varphi_r = \partial_{\mathbf{n}}\varphi_t$ for $r = a$. This gives

$$i^m n_0 J_m'(kn_0r) + n_0 R_m H_m^{'(1)}(kn_0r) - n_1 T_m J_m'(kn_1r) = 0 \tag{4.67}$$

Then there are two equations and two unknowns, hence there is a solvable system for R_m and T_m:

$$\begin{aligned}
i^m J_m(kn_0r) + R_m H_m^{(1)}(kn_0r) - T_m J_m(kn_1r) &= 0 \quad (4.68)\\
i^m n_0 J_m'(kn_0r) + n_0 R_m H_m^{'(1)}(kn_0r) - n_1 T_m J_m'(kn_1r) &= 0 \quad (4.69)
\end{aligned}$$

From these two equations, expressions for R_m and T_m are found to be the following:

$$R_m = i^m \left(\frac{n_1 J_m(kn_0r) J'_m(kn_1r) - n_0 J'_m(kn_0r) J_m(kn_1r)}{n_0 J_m(kn_1r) H_m^{'(1)}(kn_0r) - n_1 J'_m(kn_1r) H_m^{(1)}(kn_0r)} \right) \quad (4.70)$$

$$T_m = i^m n_0 \left(\frac{J_m(kn_0r) H_m^{'(1)}(kn_0r) - J'_m(kn_0r) H_m^{(1)}(kn_0r)}{n_0 J_m(kn_1r) H_m^{'(1)}(kn_0r) - n_1 J'_m(kn_1r) H_m^{(1)}(kn_0r)} \right) \quad (4.71)$$

Now all the unknowns for the wave functions are found, and it is possible to calculate $\varphi(r, \theta)$ for all points in a given domain. To summarize the results found in this section, the wave functions are as follows:

$$\varphi_i(kn_0r) = \sum_m i^m J_m(kn_0r) e^{im\theta} \quad (4.72)$$

$$\varphi_r(kn_0r) = \sum_m R_m H_m^{(1)}(kn_0r) e^{im\theta} \quad (4.73)$$

$$\varphi_t(kn_1r) = \sum_m T_m J_m(kn_1r) e^{im\theta} \quad (4.74)$$

Where R_m and T_m are given by Equations 4.70 and 4.71. For points outside the cylinder, the equation for the wave function is written as

$$\varphi(r, \theta) = \sum_m (i^m J_m(kn_0r) + R_m H_m^{(1)}(kn_0r)) e^{im\theta}, \quad (4.75)$$

while inside the cylinder, the equation for the wave function is given as

$$\varphi(r, \theta) = \sum_m T_m J_m(kn_1r) e^{im\theta} \quad (4.76)$$

The solution on the boundary of the cylinder, where $r = a$, can be calculated using any of these two equations.

So the exact solution to the Helmholtz equation for the wave function is found. The solution is calculated numerically, and the procedures used in the calculations are explained shortly in the next section. Some results for the exact solution can also be found there.

4.5 Numerical computation and results

The exact solution has been solved numerically by a program made in *Matlab*. The program is based on the equations found in this chapter. The code in its entirety can be found in Appendix A, together with some explanations to the procedures. A short description of the code will be given below together with some results.

The program uses built-in algorithms for the Bessel functions to solve the problem. The solution for the wave function, $\varphi(r, \theta)$, can be calculated

on the boundary of the cylinder, along the line $y = 0$, or for a given domain in $\mathbb{R}^2$. The equation for the wave function includes a summation over m that is supposed to go from $-\infty$ to ∞, but the series are truncated in order for computation to be possible. So the program summaries the wave function over a given interval for each point where the solution is sought.

Figure 6 shows the result for $\varphi(r, \theta)$ on the boundary of the cylinder as φ versus θ, and also an intensity plot of φ for the whole domain. In Figure 7

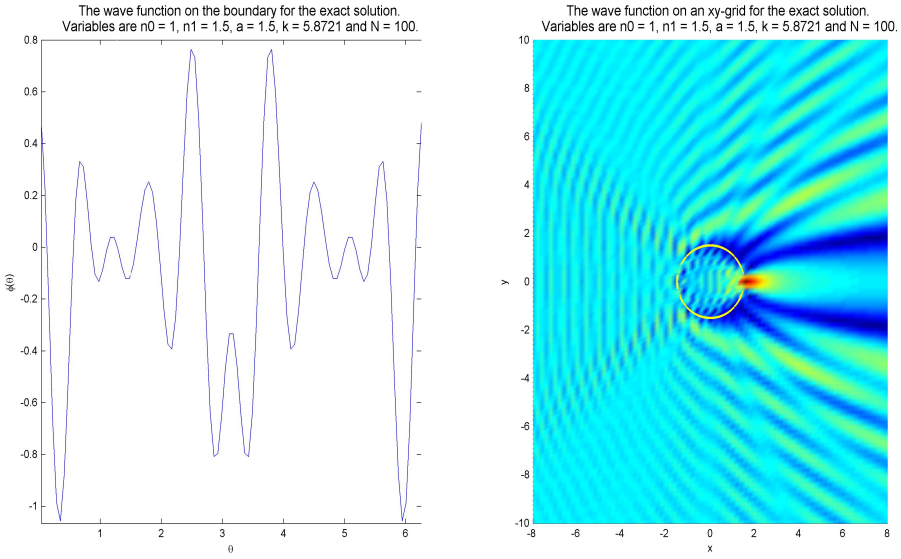

Figure 6: The left figure shows the exact solution for the wave function on the boundary of the cylinder. The right figure shows an intensity plot of the wave function for a given domain, where the cylinder is placed at the origin. The colors in the intensity plot shows the highest intensity in red, and the lowest in blue. Data used in the test can be found in the titles.

the result for the wave function is plotted along the x-axis. The edges of the cylinder are marked as stars in the figure. The value of the wave function increases significantly behind the cylinder. The same can be seen in the intensity plot in Figure 6, where the red area behind the cylinder marks the area with the highest values for the wave function.

In the next chapter an approximate solution to this problem will be derived, and the result will be compared with the exact solution that was found here in this chapter.

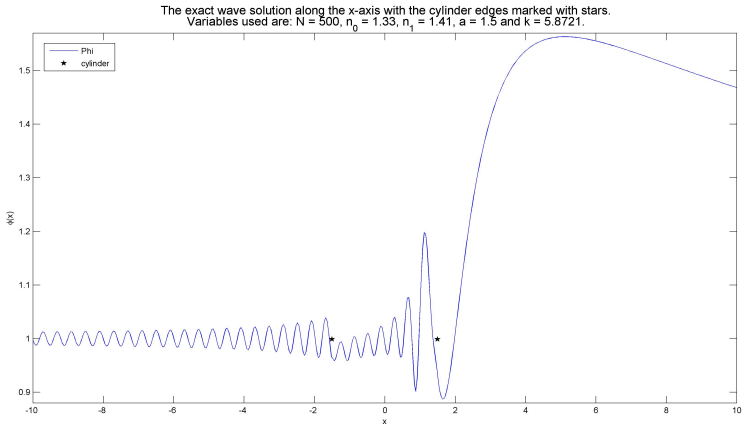

Figure 7: The exact solution for the wave function along the x-axis. The black stars mark the edges of the cylinder. Data used in the test can be found in the title.

5 Boundary Integral Method

Having found the exact solution to the wave function in the problem with one cylinder placed at the origin, the next step is to find an approximate solution to this problem. The approximate solution will be derived using the boundary integral method [6]. This method makes it possible to derive the value for the wave function $\varphi(r, \theta)$ in a given domain, just by knowing the solution to the wave function and its normal derivative on the boundary of the cylinder.

In the end of this chapter the approximative solution will be compared to the exact solution found in the previous chapter. The solutions will be compared both on the boundary of the cylinder, and for a given domain. This will show how good both the boundary integral method, and the numerical approximation are.

As for the exact solution, the Helmholtz equation found on page 11, Equation 4.22, will be used as the starting point.

5.1 Deriving the boundary integral equations

The Helmholtz equation is given as

$$\nabla^2 \varphi(\mathbf{x}) + k^2 n_j^2 \varphi(\mathbf{x}) = j(\mathbf{x}), \tag{5.1}$$

where the inhomogeneous part $j(\mathbf{x})$ is due to the source. The domain inside the cylinder is denoted as Ω and has refraction index n_1, while the domain outside the cylinder is denoted as Ω^c and has refraction index n_0.

Introducing the linear operator $\mathcal{L} = \nabla^2 + k^2 n_j^2$, the Helmholtz equation can be written as

$$\mathcal{L}\varphi(\mathbf{x}) = j(\mathbf{x}) \tag{5.2}$$

The Helmholtz equation found in Equation 5.1, is a two-dimensional differential equation that can be reduced to a one-dimensional integral equation. The first step is to introduce the Green's function, G_j, which is any solution of

$$\mathcal{L}G_j(\mathbf{x}, \zeta) = \delta(\mathbf{x} - \zeta) \tag{5.3}$$

Here $j = 0, 1$, depending on the domain (0 for Ω^c and 1 for Ω), and $\delta(\mathbf{x} - \zeta)$ is the two-dimensional Dirac delta-function. $\mathbf{x}$ and ζ are arbitrary points in $\mathbb{R}^2$. The Green's function that is sought here should satisfy the radiation condition that was given in Section 4.4.

Notice that for two different scalar functions, φ and ψ, the linear operator $\mathcal{L}$ gives:

$$\varphi\mathcal{L}\psi - \psi\mathcal{L}\varphi = \varphi(\nabla^2 + k^2 n_j^2)\psi - \psi(\nabla^2 + k^2 n_j^2)\varphi = \varphi\nabla^2\psi - \psi\nabla^2\varphi \tag{5.4}$$

And from Green's second identity [19], the following is found for an arbitrary volume V, with φ and ψ both being twice continuously differentiable in V:

$$\int_V \left(\varphi\nabla^2\psi - \psi\nabla^2\varphi\right)\, dV = \oint_{\partial V} \left(\varphi\partial_{\mathbf{n}}\psi - \psi\partial_{\mathbf{n}}\varphi\right)\, dS \tag{5.5}$$

Equations 5.4 and 5.5 then give

$$\int_V \left(\varphi\mathcal{L}\psi - \psi\mathcal{L}\varphi\right)\, dV = \oint_{\partial V} \left(\varphi\partial_{\mathbf{n}}\psi - \psi\partial_{\mathbf{n}}\varphi\right)\, dS \tag{5.6}$$

Replacing the scalar function ψ in this equation, with the Green's function introduced in Equation 5.3 yields

$$\int_V \left(\varphi\mathcal{L}G_j - G_j\mathcal{L}\varphi\right)\, dV = \oint_{\partial V} \left(\varphi\partial_{\mathbf{n}}G_j - G_j\partial_{\mathbf{n}}\varphi\right)\, dS \tag{5.7}$$

For arbitrary points inside the cylinder, that is $\zeta \in \Omega$, the equation is rewritten as

$$\begin{aligned} \int_\Omega (\varphi\mathcal{L}G_1 - G_1\mathcal{L}\varphi)\, dV &= \oint_{\partial\Omega} \left(\varphi\partial_{\mathbf{n}}G_1 - G_1\partial_{\mathbf{n}}\varphi\right)\, dS \\ \int_\Omega (\varphi(\mathbf{x})\delta(\mathbf{x} - \zeta) - G_1(\mathbf{x}, \zeta)j(\mathbf{x}))\, dV(\mathbf{x}) &= \oint_{\partial\Omega} \left(\varphi\partial_{\mathbf{n}}G_1 - G_1\partial_{\mathbf{n}}\varphi\right)\, dS \end{aligned} \tag{5.8}$$

Where $\int_\Omega \varphi(\mathbf{x})\delta(\mathbf{x} - \zeta)\, dV = \varphi(\zeta)$. The domain inside the cylinder is source free, hence $j(\mathbf{x}) = 0$ and Helmholtz's equation is homogeneous. So for arbitrary points $\zeta \in \Omega$ and $\mathbf{x} \in \partial\Omega$, the identity for $\varphi(\zeta)$ is given as

$$\varphi(\zeta) = \oint_{\partial\Omega} \left(\varphi(\mathbf{x})\partial_{\mathbf{n}}G_1(\mathbf{x}, \zeta) - G_1(\mathbf{x}, \zeta)\partial_{\mathbf{n}}\varphi(\mathbf{x})\right)\, dS(\mathbf{x}) \tag{5.9}$$

For the domain outside the cylinder, the source makes the Helmholtz equation inhomogeneous with $j(\mathbf{x}) \neq 0$. For this domain Equation 5.7 gives

$$\begin{aligned} \int_{\Omega^c} (\varphi \mathcal{L} G_0 - G_0 \mathcal{L}\varphi)\, dV &= -\oint_{\partial\Omega} (\varphi \partial_{\mathbf{n}} G_0 - G_0 \partial_{\mathbf{n}}\varphi)\, dS \\ \int_{\Omega^c} (\varphi(\mathbf{x})\delta(\mathbf{x}-\zeta) - G_0(\mathbf{x},\zeta) j(\mathbf{x}))\, dV(\mathbf{x}) &= -\oint_{\partial\Omega} (\varphi \partial_{\mathbf{n}} G_0 - G_0 \partial_{\mathbf{n}}\varphi)\, dS \end{aligned} \quad (5.10)$$

The minus signs in front of the boundary integrals are due to the orientation of the normal vector. The normal vector for the domain outside the cylinder points in the opposite direction to the normal vector for the domain inside the cylinder, see Figure 8. The normal vector for the domain outside the cylinder is set to be in the negative direction, which leads to the minus signs in the equations. So, for arbitrary points $\zeta \in \Omega^c$ and $\mathbf{x} \in \partial\Omega$, the identity for $\varphi(\zeta)$ is given as

$$\varphi(\zeta) = \int_{\Omega^c} G_0(\mathbf{x},\zeta) j(\mathbf{x})\, dV(\mathbf{x}) - \oint_{\partial\Omega} (\varphi(\mathbf{x}) \partial_{\mathbf{n}} G_0(\mathbf{x},\zeta) - G_0(\mathbf{x},\zeta)\partial_{\mathbf{n}}\varphi(\mathbf{x}))\, dS(\mathbf{x}) \quad (5.11)$$

Figure 8: The illustration shows the orientation of the normal vector. For the domain inside the cylinder, Ω, the normal vector points outwards (left figure), while the normal vector for the domain outside the cylinder, Ω^c, points inwards (right figure). The outwards direction has been set to be the positive one.

The volume integral in the equation above is the particular solution to the Helmholtz equation when $j(\mathbf{x}) \neq 0$ and $n(\mathbf{x}) = n_0$. $\varphi_i(\zeta)$ is the field at ζ generated by the source in the absence of the scattering object. This is by definition the initial field, hence it is replaced for the particular solution, and the identity for the wave function simplifies to

$$\varphi(\zeta) = \varphi_i(\zeta) - \oint_{\partial\Omega} (\varphi(\mathbf{x}) \partial_{\mathbf{n}} G_0(\mathbf{x},\zeta) - G_0(\mathbf{x},\zeta)\partial_{\mathbf{n}}\varphi(\mathbf{x}))\, dS(\mathbf{x}) \quad (5.12)$$

Two identities for $\varphi(\zeta)$ are now found, one for $\zeta \in \Omega^c$ and one for $\zeta \in \Omega$. The two identities are summarized in Equations 5.13 and 5.14. In both cases $\mathbf{x}$ is on the boundary of the cylinder, $\mathbf{x} \in \partial\Omega$, while ζ is either inside the cylinder, or in the complement domain, Ω^c. To find equations for $\varphi(\zeta)$, ζ

needs to approach the boundary $\partial\Omega$ from the outside and from the inside for Equations 5.13 and 5.14 respectively. This will be done in the next section.

$$\varphi(\zeta) = \varphi_i(\zeta) - \oint_{\partial\Omega} (\varphi(\mathbf{x})\partial_{\mathbf{n}} G_0(\mathbf{x},\zeta) - G_0(\mathbf{x},\zeta)\partial_{\mathbf{n}}\varphi(\mathbf{x}))\, dS(\mathbf{x}), \quad \zeta \in \Omega^c \tag{5.13}$$

$$\varphi(\zeta) = \oint_{\partial\Omega} (\varphi(\mathbf{x})\partial_{\mathbf{n}} G_1(\mathbf{x},\zeta) - G_1(\mathbf{x},\zeta)\partial_{\mathbf{n}}\varphi(\mathbf{x}))\, dS(\mathbf{x}), \quad \zeta \in \Omega \tag{5.14}$$

5.2 The wave function φ on the boundary $\partial\Omega$

The goal now is to find equations for $\varphi(\zeta)$ on the boundary of the cylinder. To find these equations, the analytic expressions for the Green's function, $G_j(\mathbf{x},\zeta)$, and its normal derivative, $\partial_{\mathbf{n}} G_j(\mathbf{x},\zeta)$, are needed. They will be derived next.

5.2.1 The Green's function

The Green's function is a type of function that can be used to solve inhomogeneous differential equations with some given boundary conditions [11].

The first part of the calculation is to move the origin of the coordinate system to the point $\mathbf{x}$, define a new vector $\mathbf{R} = \mathbf{x} - \zeta$, and then take the two-dimensional fourier transform [20] of the Green's function, G_j, which gives

$$\hat{G}_j(\mathbf{q}) = \int_{-\infty}^{\infty}\int_{-\infty}^{\infty} G_j(\mathbf{R}) e^{-i\mathbf{q}\cdot\mathbf{R}}\, d\mathbf{R} \tag{5.15}$$

Here $\mathbf{q} = (x', y')$ and $\mathbf{R} = (x, y)$. The inverse Fourier transform is given as [20]

$$G_j(\mathbf{R}) = \left(\frac{1}{2\pi}\right)^2 \int_{-\infty}^{\infty}\int_{-\infty}^{\infty} \hat{G}_j(\mathbf{q}) e^{i\mathbf{q}\cdot\mathbf{R}}\, d\mathbf{q} \tag{5.16}$$

Taking the Fourier transform of the Helmholtz equation for the Green's function, given as $(\nabla^2_{\mathbf{x}} + k^2 n_j^2) G_j(\mathbf{R}) = \delta(\mathbf{R})$, leads to

$$(k^2 n_j^2 - x'^2 - y'^2)\hat{G}_j(\mathbf{q}) = 1 \tag{5.17}$$

Now, changing to polar coordinates by setting $\mathbf{q} = (\rho\cos(\theta), \rho\sin(\theta))$, $\mathbf{R} = (R\cos(\vartheta), R\sin(\vartheta))$, and $dx\, dy = \rho\, d\theta$, and then replacing the fourier transform of Green's function in Equation 5.16 with the expression found in Equation 5.17 yields

$$G_j(R,\vartheta) = \left(\frac{1}{2\pi}\right)^2 \int_0^{\infty} \frac{1}{-\rho^2 + k^2 n_j^2} \int_0^{2\pi} e^{i\rho R(\cos(\theta)\cos(\vartheta) + \sin(\theta)\sin(\vartheta))}\, \rho\, d\theta\, d\rho \tag{5.18}$$

By utilizing the formula for angle addition given in Equation 4.55 on page 17, and also changing the angle variable to $\theta' = \theta - \vartheta$ which does not change the final result, the Green's function simplifies to

$$G_j(R,\vartheta) = -\left(\frac{1}{2\pi}\right)^2 \int_0^\infty \frac{\rho}{\rho^2 - k^2 n_j^2} \int_0^{2\pi} e^{i\rho R\cos(\theta)}\, d\theta\, d\rho \tag{5.19}$$

The Bessel function of the first kind and zeroth order can be given as the integral [11],

$$J_0(z) = \frac{1}{2\pi} \int_0^{2\pi} e^{iz\cos(\theta)}\, d\theta, \tag{5.20}$$

which resembles the latter integral of Equation 5.19. The Green's function is rewritten as

$$G_j(R,\vartheta) = -\frac{1}{2\pi} \int_0^\infty \frac{\rho J_0(\rho R)}{\rho^2 - k^2 n_j^2}\, d\rho \tag{5.21}$$

To avoid the singularity for $\rho = \pm k n_j$ in the equation, an infinitely small, positive imaginary part, ϵ, will be added to kn_j, i.e., $kn_j \to kn_j + i\epsilon$. This gives $k^2 n_j^2 \to (kn_j + i\epsilon)^2 = -(\epsilon - ikn_j)^2$ [8]. In addition the modified Bessel function of the second kind is given as [21]

$$K_0(\alpha k n_j) = \int_0^\infty \frac{x J_0(\alpha x)}{x^2 + k^2 n_j^2}\, dx \tag{5.22}$$

And so the equation for the Green's function changes to

$$\begin{aligned} G_j(R,\vartheta) &= -\frac{1}{2\pi} \lim_{\epsilon\to\infty} \int_0^\infty \frac{\rho J_0(R\rho)}{\rho^2 + (\epsilon - ikn_j)^2}\, d\rho = -\frac{1}{2\pi} \lim_{\epsilon\to\infty} K_0(R(\epsilon - ikn_j)) \\ &= -\frac{1}{2\pi} K_0(-ikn_j R) \end{aligned} \tag{5.23}$$

Finally the modified Bessel function of the second kind, K_0, relates to the Hankel function of the first kind the following way: $K_m(z) = \frac{\pi}{2} i^{m+1} H_m^{(1)}(iz)$ [22]. From this, the Green's function for the two-dimensional Helmholtz equation is simplified to

$$G_j(\mathbf{x},\zeta) = -\frac{i}{4} H_0^{(1)}(kn_j\, ||\mathbf{x} - \zeta||) \tag{5.24}$$

The solution satisfies the radiation condition found on page 15.

Then the normal derivative for the Green's function can be derived. A directional derivative for a function, f, is given as $\partial_{\mathbf{v}} f = \nabla f \cdot \mathbf{v}$, $\mathbf{v}$ being

the direction in which the derivative is taken [19]. The vectors $\mathbf{x}$ and ζ are written as $\mathbf{x} = (x, y)$ and $\zeta = (x', y')$, and the derivative of the Hankel function of order zero is given as $\partial_z H_0^{(1)}(z) = -H_1^{(1)}(z)$ [16]. Hence the normal derivative of the Green's function is derived in the following way

$$\begin{aligned}
\partial_{\mathbf{n}} G_j(\mathbf{x}, \zeta) &= \nabla_{\mathbf{x}} \left(-\frac{i}{4} H_0^{(1)}(kn_j \, ||\mathbf{x} - \zeta||) \right) \cdot \mathbf{n}(\mathbf{x}) \\
&= \frac{ikn_j}{4} H_1^{(1)}(kn_j \, ||\mathbf{x} - \zeta||) \nabla_{\mathbf{x}}(||\mathbf{x} - \zeta||) \cdot \mathbf{n}(\mathbf{x}) \\
&= \frac{ikn_j}{4} H_1^{(1)}(kn_j \, ||\mathbf{x} - \zeta||) \left[\frac{2(x - x') + 2(y - y')}{2\sqrt{((x - x')^2 + (y - y')^2)}} \right] \cdot \mathbf{n}(\mathbf{x}) \\
&= \frac{ikn_j}{4} H_1^{(1)}(kn_j \, ||\mathbf{x} - \zeta||) \frac{\mathbf{x} - \zeta}{||\mathbf{x} - \zeta||} \cdot \mathbf{n}(\mathbf{x}) \qquad (5.25)
\end{aligned}$$

So now the Green's function and its normal derivative are found, and the solutions are summarized below

$$G_j(\mathbf{x}, \zeta) = -\frac{i}{4} H_0^{(1)}(kn_j \, ||\mathbf{x} - \zeta||) \qquad (5.26)$$

$$\partial_{\mathbf{n}} G_j(\mathbf{x}, \zeta) = \frac{\mathbf{x} - \zeta}{||\mathbf{x} - \zeta||} \cdot \mathbf{n}(\mathbf{x}) \frac{ikn_j}{4} H_1^{(1)}(kn_j \, ||\mathbf{x} - \zeta||) \qquad (5.27)$$

5.2.2 Principle value integrals

Having found both the Green's function and its normal derivative, the next step will be to let $\zeta \in \Omega$ and $\zeta \in \Omega^c$ approach the boundary $\partial\Omega$. A problem occurs when $||\zeta - \mathbf{x}|| \to 0$, due to the characteristic of the Hankel functions, which the Green's function and its normal derivative are based on. For small arguments the Hankel functions of the zeroth and first order are given as [16]

$$\lim_{z \to 0} H_0^{(1)}(z) \approx \frac{2i}{\pi} \log(z) \qquad \lim_{z \to 0} H_1^{(1)}(z) \approx -\frac{2i}{z\pi} \qquad (5.28)$$

Hence for small arguments, the Green's function and its normal derivative are both singular. This situation will occur when ζ approaches $\mathbf{x}$. However, both integral equations for $\varphi(\zeta)$ are still integrable in the sense of Cauchy's principal value integral (PV). A principal value integral is given as [8]

$$\lim_{\epsilon \to 0} \int_{\mathcal{S}_\epsilon} dS(\mathbf{x}) = PV \int_{\mathcal{S}} dS(\mathbf{x}) \qquad (5.29)$$

Where the contour $\mathcal{S}_\epsilon$ approaches the closed contour $\mathcal{S}$ when $\epsilon \to 0$. For the problem at hand, the contour $\mathcal{S}_\epsilon$, or actually $\mathcal{S}_\epsilon + \mathcal{C}_\epsilon$, will have a semicircle with radius ϵ at the point on the boundary where $\zeta = \mathbf{x}$, see Figure 9. The contour $\mathcal{C}_\epsilon$ is the part that goes around the semicircle, while $\mathcal{S}_\epsilon$ is the rest of the boundary. The semicircle is very small as $\epsilon \to 0$, and due to this it is

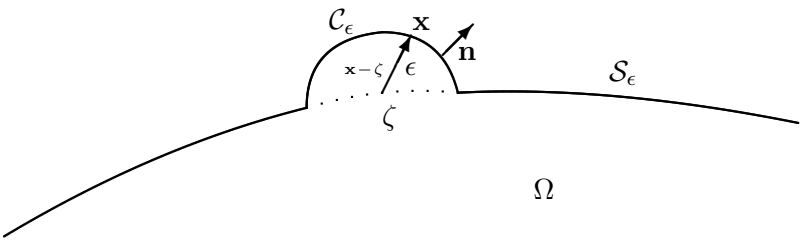

Figure 9: A semicircle is made on the boundary of the cylinder where $||\mathbf{x}-\zeta|| \to 0$. This has been done to avoid the singularity in the Green's function and its normal derivative at this point. The semicircle is very small and is assumed not to have any influence on the scattering of a wave.

assumed that the semicircle will not have any influence on the scattering of the wave.

The semicircle will now be introduced to the identities for φ, starting with the domain inside the cylinder. The identity for the wave function in this domain was found in Equation 5.14 on page 24 as

$$\varphi(\zeta) = \int_{\partial\Omega} (\varphi(\mathbf{x})\partial_{\mathbf{n}}G_1(\mathbf{x},\zeta) - G_1(\mathbf{x},\zeta)\partial_{\mathbf{n}}\varphi(\mathbf{x}))\, dS(\mathbf{x}), \quad \zeta \in \Omega \tag{5.30}$$

Now, the semicircle arises by replacing the boundary $\partial\Omega$ by the contour $\mathcal{C}_\epsilon + \mathcal{S}_\epsilon$. The first part of the integral in the above equation can then be rewritten as

$$\int_{\partial\Omega} (\varphi\partial_{\mathbf{n}}G_1)\, dS = \int_{\mathcal{S}_\epsilon} (\varphi\partial_{\mathbf{n}}G_1)\, dS + \int_{\mathcal{C}_\epsilon} (\varphi\partial_{\mathbf{n}}G_1)\, dS \tag{5.31}$$

The $\mathbf{x}$-value follows the semicircle and is given as $\mathbf{x} = \zeta + \epsilon e^{i\theta}$, where the angle is defined as $0 \le \theta \le \pi$. The most interesting part in the equation above is the integral over $\mathcal{C}_\epsilon$. By replacing the normal derivative $\partial_{\mathbf{n}}G_1$, with the expression found in Equation 5.27, the integral over the semicircle becomes

$$\int_{\mathcal{C}_\epsilon} (\varphi\partial_{\mathbf{n}}G_1)\, dS = \frac{ikn_1}{4} \int_0^\pi \frac{\mathbf{x}-\zeta}{||\mathbf{x}-\zeta||} \cdot \mathbf{n}(\mathbf{x})\, H_1^{(1)}(kn_1\epsilon)\varphi(\zeta+\epsilon e^{i\theta})\epsilon\, d\theta \tag{5.32}$$

Where $\frac{\mathbf{x}-\zeta}{||\mathbf{x}-\zeta||} \cdot \mathbf{n}(\mathbf{x}) = 1$ as $\epsilon \to 0$, and $\varphi(\zeta + \epsilon e^{i\theta}) \to \varphi(\zeta)$. Hence the equation can be rewritten as

$$\int_{\mathcal{C}_\epsilon} (\varphi\partial_{\mathbf{n}}G_1)\, dS \approx \frac{ikn_1\epsilon}{4} H_1^{(1)}(kn_1\epsilon)\varphi(\zeta)\pi \tag{5.33}$$

Using the approximation of the first order Hankel function for small arguments, found in Equation 5.28, the integral over $\mathcal{C}_\epsilon$ simplifies to

$$\int_{\mathcal{C}_\epsilon} (\varphi \partial_{\mathbf{n}} G_1)\ dS \approx \frac{ikn_1\epsilon}{4}\frac{-2i}{kn_1\epsilon\pi}\varphi(\zeta)\pi = \frac{1}{2}\varphi(\zeta) \tag{5.34}$$

So as $\epsilon \to 0$, the contour $\mathcal{C}_\epsilon + \mathcal{S}_\epsilon$ approaches the boundary $\partial\Omega$ and gives

$$\lim_{\epsilon\to 0}\int_{\mathcal{S}_\epsilon+\mathcal{C}_\epsilon} (\varphi \partial_{\mathbf{n}} G_1)\ dS = PV\int_{\partial\Omega} (\varphi \partial_{\mathbf{n}} G_1)\ dS + \frac{1}{2}\varphi(\zeta) \tag{5.35}$$

Now the same procedure is performed on the second part of the integral in Equation 5.30. First the semicircle is introduced with the new contour $\mathcal{C}_\epsilon + \mathcal{S}_\epsilon$ to give

$$\int_{\partial\Omega} (G_1 \partial_{\mathbf{n}} \varphi)\ dS = \int_{\mathcal{S}_\epsilon} (G_1 \partial_{\mathbf{n}} \varphi)\ dS + \int_{\mathcal{C}_\epsilon} (G_1 \partial_{\mathbf{n}} \varphi)\ dS \tag{5.36}$$

Again the $\mathbf{x}$-value is given as $\mathbf{x} = \zeta + \epsilon e^{i\theta}$, and $0 \le \theta \le \pi$. Using the Green's function found in Equation 5.26, the integral for $\mathcal{C}_\epsilon$ turns out to be

$$\int_{\mathcal{C}_\epsilon} (G_1 \partial_{\mathbf{n}} \varphi)\ dS = -\frac{i}{4}\int_0^\pi H_0^{(1)}(kn_1\epsilon)\partial_{\mathbf{n}}\varphi(\zeta + \epsilon e^{i\theta})\epsilon\, d\theta \tag{5.37}$$

And as $\epsilon \to 0$, $\partial_{\mathbf{n}}\varphi(\zeta + \epsilon e^{i\theta}) \to \partial_{\mathbf{n}}\varphi(\zeta)$. Now recall the approximation of the zeroth order Hankel function for small arguments, found in Equation 5.28, which simplifies the integral over the semicircle to

$$\begin{aligned}\int_{\mathcal{C}_\epsilon} (G_1 \partial_{\mathbf{n}} \varphi)\ dS &\approx -\frac{i}{4}\frac{2i}{\pi}\log(kn_1\epsilon)\partial_{\mathbf{n}}\varphi(\zeta)\epsilon\pi \\ &= \frac{\epsilon}{2}\log(kn_1\epsilon)\partial_{\mathbf{n}}\varphi(\zeta) = 0\end{aligned} \tag{5.38}$$

Hence, there is no contribution from the semicircle, and the limit when ϵ approaches zero will be just the principal value integral itself:

$$\lim_{\epsilon\to 0}\int_{\mathcal{S}_\epsilon+\mathcal{C}_\epsilon} (G_1 \partial_{\mathbf{n}} \varphi)\ dS = PV\int_{\partial\Omega} (G_1 \partial_{\mathbf{n}} \varphi)\ dS \tag{5.39}$$

Replacing the integrals in Equation 5.30 with the principal value integrals found in Equations 5.35 and 5.39 give

$$\varphi(\zeta) = PV\int_{\partial\Omega} \varphi \partial_{\mathbf{n}} G_1 + \frac{1}{2}\varphi(\zeta) - PV\int_{\partial\Omega} G_1 \partial_{\mathbf{n}}\varphi\, dS \tag{5.40}$$

Hence the equation for $\varphi(\zeta)$ with ζ, $\mathbf{x} \in \partial\Omega$, is given as

$$\frac{1}{2}\varphi(\zeta) = PV\int_{\partial\Omega}\Big(\varphi(\mathbf{x})\partial_{\mathbf{n}} G_1(\mathbf{x},\zeta) - G_1(\mathbf{x},\zeta)\partial_{\mathbf{n}}\varphi(\mathbf{x})\Big)\, dS(\mathbf{x}) \tag{5.41}$$

Now there is one equation and two unknowns, namely φ and $\partial_{\mathbf{n}}\varphi$. One more equation is needed to solve the system.

The second equation is found by letting ζ approach the boundary $\partial\Omega$ from the outside. For this situation the semicircle will go inwards, see Figure 10. Still the semicircle is so small that even though it goes inwards, it is assumed that it will not have any influence on the scattering of the wave. The identity for $\varphi(\zeta)$ with $\zeta \in \Omega^c$, was found in Equation 5.13 on page 24 as

$$\varphi(\zeta) = \varphi_i(\zeta) - \int_{\partial\Omega} (\varphi(\mathbf{x})\partial_{\mathbf{n}}G_0(\mathbf{x},\zeta) - G_0(\mathbf{x},\zeta)\partial_{\mathbf{n}}\varphi(\mathbf{x}))\, dS(\mathbf{x}) \tag{5.42}$$

The semicircle is introduced to the first part of the integral in this identity

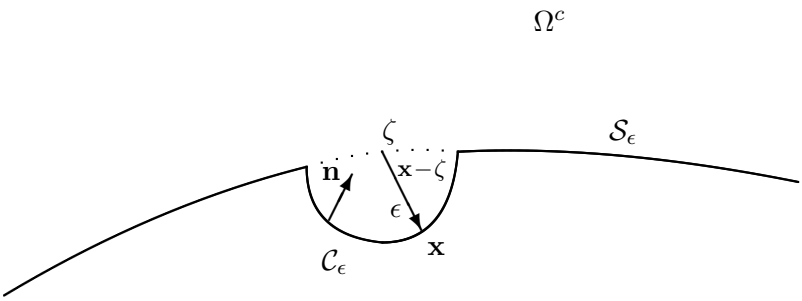

Figure 10: "Inwards" semicircle on the boundary of the cylinder where $||\mathbf{x}-\zeta|| \to 0$. The semicircle has been made to avoid the singularities that arise for the Green's function and its normal derivative when $\mathbf{x} = \zeta$. The semicircle is so small that it is assumed not to have any influence on the scattering of a wave.

to give

$$\int_{\partial\Omega} (\varphi\partial_{\mathbf{n}}G_0)\, dS = \int_{\mathcal{S}_\epsilon} (\varphi\partial_{\mathbf{n}}G_0)\, dS + \int_{\mathcal{C}_\epsilon} (\varphi\partial_{\mathbf{n}}G_0)\, dS \tag{5.43}$$

So for $\mathbf{x}$ to follow the semicircle, set $\mathbf{x} = \zeta - \epsilon e^{i\theta}$, and $-\pi \le \theta \le 0$. Using the expression for the normal derivative of the Green's function, found in Equation 5.27, gives the following for the integral over $\mathcal{C}_\epsilon$

$$\int_{\mathcal{C}_\epsilon} (\varphi\partial_{\mathbf{n}}G_0)\, dS = \frac{ikn_0}{4} \int_{-\pi}^{0} \frac{\mathbf{x}-\zeta}{||\mathbf{x}-\zeta||} \cdot \mathbf{n}(\mathbf{x})\, H_1^{(1)}(kn_0\epsilon)\varphi(\zeta - \epsilon e^{i\theta})\epsilon\, d\theta \tag{5.44}$$

Where $\frac{\mathbf{x}-\zeta}{||\mathbf{x}-\zeta||} \cdot \mathbf{n}(\mathbf{x}) = -1$ since $\mathbf{x}-\zeta$ points in the opposite direction as the normal vector, see Figure 10. As $\epsilon \to 0$, $\varphi(\zeta - \epsilon e^{i\theta}) \to \varphi(\zeta)$. This together with the approximation for the Hankel functions for small arguments, found in Equation 5.28 on page 26, gives

$$\int_{\mathcal{C}_\epsilon} (\varphi \partial_{\mathbf{n}} G_0)\, dS \approx \frac{-ikn_0}{4} \frac{-2i}{kn_0\epsilon\pi} \varphi(\zeta)\epsilon\pi = -\frac{1}{2}\varphi(\zeta) \tag{5.45}$$

And Equation 5.43 is then rewritten as

$$\lim_{\epsilon\to 0} \int_{\mathcal{S}_\epsilon + \mathcal{C}_\epsilon} (\varphi \partial_{\mathbf{n}} G_0)\, dS = PV \int_{\partial\Omega} (\varphi \partial_{\mathbf{n}} G_0)\, dS - \frac{1}{2}\varphi(\zeta) \tag{5.46}$$

Now the same procedure is performed on the second part of the surface integral in Equation 5.42. The semicircle is introduced and the new contour $\mathcal{C}_\epsilon + \mathcal{S}_\epsilon$ replaces the boundary $\partial\Omega$

$$\int_{\partial\Omega} (G_0 \partial_{\mathbf{n}} \varphi)\, dS = \int_{\mathcal{S}_\epsilon} (G_0 \partial_{\mathbf{n}} \varphi)\, dS + \int_{\mathcal{C}_\epsilon} (G_0 \partial_{\mathbf{n}} \varphi)\, dS \tag{5.47}$$

As before $\mathbf{x} = \zeta - \epsilon e^{i\theta}$, and $-\pi \le \theta \le 0$. Replacing G_0 with the expression for the Green's function, found in Equation 5.26, gives the following for the integration over the semicircle

$$\int_{\mathcal{C}_\epsilon} (G_0 \partial_{\mathbf{n}} \varphi)\, dS = -\frac{i}{4} \int_0^\pi H_0^{(1)}(kn_0\epsilon) \partial_{\mathbf{n}} \varphi(\zeta - \epsilon e^{i\theta}) \epsilon\, d\theta \tag{5.48}$$

Letting ϵ approach zero, $\varphi(\zeta - \epsilon e^{i\theta}) \to \varphi(\zeta)$. Then by replacing the Hankel function with the approximation for small arguments, the integral over the contour $\mathcal{C}_\epsilon$ will be

$$\begin{aligned} \int_{\mathcal{C}_\epsilon} (G_0 \partial_{\mathbf{n}} \varphi)\, dS &\approx -\frac{i}{4}\frac{2i}{\pi} \log(kn_0\epsilon) \partial_{\mathbf{n}} \varphi(\zeta)\epsilon\pi \\ &= \frac{\epsilon}{2} \log(kn_0\epsilon) \partial_{\mathbf{n}} \varphi(\zeta) \ = 0 \end{aligned} \tag{5.49}$$

So there is no contribution from the semicircle, and the limit when ϵ approaches zero will be just the principal value integral itself.

$$\lim_{\epsilon\to 0} \int_{\mathcal{S}_\epsilon + \mathcal{C}_\epsilon} (G_0 \partial_{\mathbf{n}} \varphi)\, dS = PV \int_{\partial\Omega} (G_0 \partial_{\mathbf{n}} \varphi)\, dS \tag{5.50}$$

Hence a new equation for $\varphi(\zeta)$, with ζ, $\mathbf{x} \in \partial\Omega$, is given as

$$\begin{aligned} \varphi(\zeta) &= \varphi_i(\zeta) - PV \int_{\partial\Omega} \varphi \partial_{\mathbf{n}} G_0\, dS + \frac{1}{2}\varphi(\zeta) + PV \int_{\partial\Omega} G_0 \partial_{\mathbf{n}} \varphi\, dS \\ \frac{1}{2}\varphi(\zeta) &= \varphi_i(\zeta) - PV \int_{\partial\Omega} \Big(\varphi(\mathbf{x}) \partial_{\mathbf{n}} G_0(\mathbf{x},\zeta) - G_0(\mathbf{x},\zeta) \partial_{\mathbf{n}} \varphi(\mathbf{x}) \Big)\, dS(\mathbf{x}) \end{aligned} \tag{5.51}$$

Finally there are two equations for two unknowns, and the system is solvable. The unknowns are φ and $\partial_{\mathbf{n}}\varphi$ on the boundary of the cylinder, and the equations are given as

$$\frac{1}{2}\varphi(\zeta) = \oint_{\partial\Omega}\Big(\varphi(\mathbf{x})\partial_{\mathbf{n}}G_1(\mathbf{x},\zeta) - G_1(\mathbf{x},\zeta)\partial_{\mathbf{n}}\varphi(\mathbf{x})\Big)\,dS(\mathbf{x}) \tag{5.52}$$

$$\frac{1}{2}\varphi(\zeta) = \varphi_i(\zeta) - \oint_{\partial\Omega}\Big(\varphi(\mathbf{x})\partial_{\mathbf{n}}G_0(\mathbf{x},\zeta) - G_0(\mathbf{x},\zeta)\partial_{\mathbf{n}}\varphi(\mathbf{x})\Big)\,dS(\mathbf{x}) \tag{5.53}$$

With ζ, $\mathbf{x} \in \partial\Omega$. From these two equations the unknowns will be found by numerical approximation using a program made in *Matlab*. More about this in Section 5.4. First the equations for calculating the wave function for the whole domain will be derived.

5.3 The wave function for the whole domain

The boundary integral method uses the solution of the wave function and its normal derivative on the boundary of the cylinder, to calculate the wave function for the whole domain [6]. Now, recall the identities for the wave function found in the end of Section 5.1 given as

$$\varphi(\zeta) = \varphi_i(\zeta) - \oint_{\partial\Omega}\left(\varphi(\mathbf{x})\partial_{\mathbf{n}}G_0(\mathbf{x},\zeta) - G_0(\mathbf{x},\zeta)\partial_{\mathbf{n}}\varphi(\mathbf{x})\right)\,dS(\mathbf{x}),\ \zeta \in \Omega^c \tag{5.54}$$

$$\varphi(\zeta) = \oint_{\partial\Omega}\left(\varphi(\mathbf{x})\partial_{\mathbf{n}}G_1(\mathbf{x},\zeta) - G_1(\mathbf{x},\zeta)\partial_{\mathbf{n}}\varphi(\mathbf{x})\right)\,dS(\mathbf{x}),\ \zeta \in \Omega \tag{5.55}$$

All the variables on the right hand side of these two equations are known from the last section. Hence, after calculating the unknown values for φ and $\partial_{\mathbf{n}}\varphi$ on the boundary of the cylinder, the two equations above are used for calculating the wave function for any ζ. That is the beauty of the boundary integral method, which makes it easy to find $\varphi(\zeta)$ for a whole domain, as long as the values on the boundary are known. As for the values on the boundary, the values for the wave function in the domain will be calculated in *Matlab*.

5.4 Numerical computations and results

The calculation of the boundary values for the wave function φ, and its normal derivative $\partial_{\mathbf{n}}\varphi$, is computed numerically by a program made in *Matlab*. These values are then used further in the program to calculate the wave function for a given domain. A short explanation to the procedures will be mentioned here, but the code in its entirety and a more detailed description of the code can be found in Appendix B.

5.4.1 The numerical algorithm

The equations for the wave function on the boundary of the cylinder are solved numerically by building a matrix $\mathbf{M}$, two vectors $\mathbf{X}$ and $\mathbf{b}$, and then solving the equation $\mathbf{MX} = \mathbf{b}$ by a so-called *matrix left division* in *Matlab*: $\mathbf{X} = \mathbf{M}\backslash\mathbf{b}$. *Matlab* executes the calculation as a Gaussian elimination [23].

The matrix $\mathbf{M}$ is a block-matrix that is build up from Equations 5.52 and 5.53. It contains the values for the Green's function and its normal derivative on the boundary of the cylinder. This results in a 2×2 block-matrix:

$$\mathbf{M} = \begin{pmatrix} \partial_{\mathbf{n}} G_0 & G_0 \\ \partial_{\mathbf{n}} G_1 & G_1 \end{pmatrix} \tag{5.56}$$

The elements in each block represents all the different combinations for the variables $\mathbf{x}$ and ζ on the boundary of the cylinder.

The first half of vector $\mathbf{b}$ contains the known incident wave function φ_i, which is found in the equation for the domain outside the cylinder. The rest of $\mathbf{b}$ is filled up with zeros. Then there is vector $\mathbf{X}$, which is the unknown vector representing the φ's and $\partial_{\mathbf{n}}\varphi$'s that are sought. By performing the matrix left division mentioned above, the unknown values on the boundary are found.

Having found the values on the boundary of the cylinder, due to the beauty of the boundary integral method, $\varphi(\zeta)$ can easily be calculated for all ζ in the domain, using Equations 5.54 and 5.55. In the program, $\varphi(\zeta)$ for the cylinder is calculated from the following dot product of two vectors

$$\varphi(\zeta) = \begin{bmatrix} \partial_{\mathbf{n}} G_1 \\ G_1 \end{bmatrix} \cdot \begin{bmatrix} \varphi \\ \partial_{\mathbf{n}} \varphi \end{bmatrix} \tag{5.57}$$

Another dot product calculates $\varphi(\zeta)$ for ζ outside the cylinder to be

$$\varphi(\zeta) = \varphi_i(\zeta) - \begin{bmatrix} \partial_{\mathbf{n}} G_0 \\ G_0 \end{bmatrix} \cdot \begin{bmatrix} \varphi \\ \partial_{\mathbf{n}} \varphi \end{bmatrix} \tag{5.58}$$

In both cases, the G_j's and $\partial_{\mathbf{n}} G_j$'s are vectors representing the Green's function and its normal derivative for one value of ζ and all the corresponding values of $\mathbf{x}$. Hence they are vectors the same length as the number of points found on the boundary of the cylinder. The vectors represented by φ and $\partial_{\mathbf{n}}\varphi$ in the equations above have the same length, and contains the values for the wave function and its normal derivative in each point on the boundary. A more detailed description of the program can be found in Appendix B.

5.4.2 Compare result with exact solution

The numerical solution of the boundary integral method, and the exact solution found in Chapter 4, will now be compared to see how good the approximative method is. Figure 11 shows the exact solution and the numerical

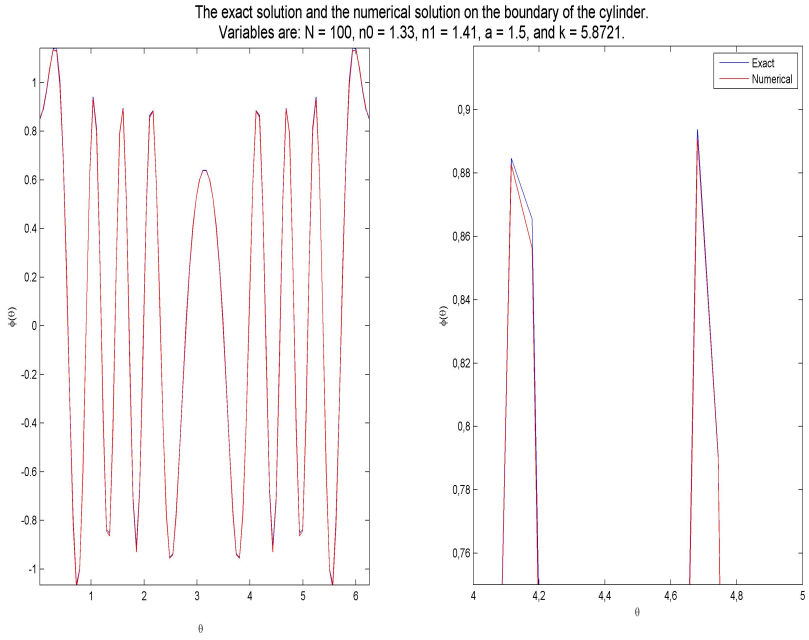

Figure 11: The exact solution compared to the numerical solution on the boundary of the cylinder. The two solutions are hard to separate from each other, but a part of the plot has been magnified on the right side to be able to see a difference. Data from the test can be found in the titles.

solution on the boundary of the cylinder. The two graphs seem to cover each other almost completely. The difference is visible only by magnifying a part of the graph (see the right plot in the figure). The mean difference of the real values for the two solutions is found to be in the order of 10^{-3}, and the maximum absolute difference for the real values is found to be about 10^{-2}. These numbers, in addition to the figure, show that the two solutions are quite similar, even with a fairly low number of grid-points on the boundary (100 points are used here). The conclusion is that the numerical solution is found to be close to the exact solution on the boundary.

The exact and the numerical solutions are also compared to each other for the wave function along the x-axis. This can be seen in Figure 12. The two graphs follow each other quite well except for the spikes that arise on the boundary of the cylinder for the numerical solution. Some difference is also seen inside the cylinder.

Finally the two solutions are compared to each other by intensity plots of the wave function for the whole domain. This comparison gives an idea on the accuracy of the boundary integral method, which is used for the calculation. The total error in the approximative solution also includes

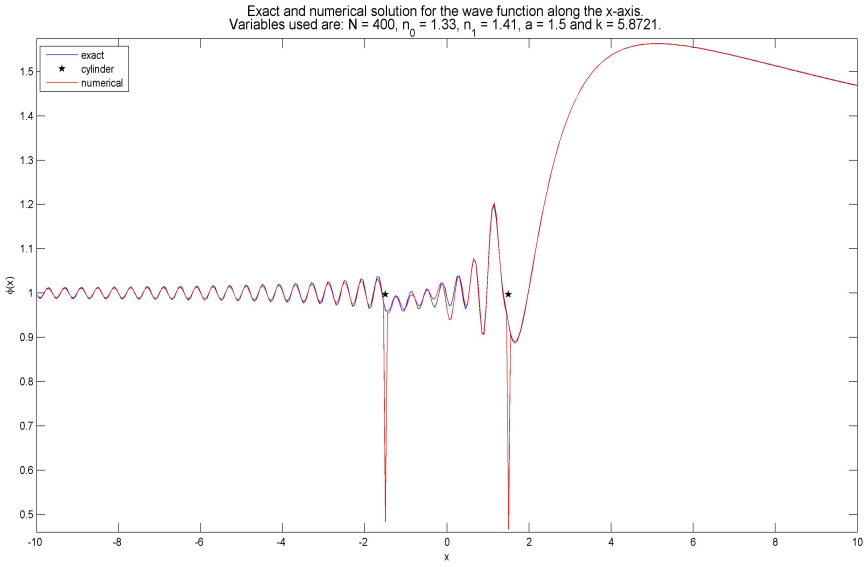

Figure 12: The exact and the numerical solution for the wave function along the x-axis are compared in the figure. The numerical solution has some irregularities on the boundary of the cylinder due to the characteristics of the Hankel functions. Outside the cylinder the two solutions follow each other quite well, but some differences can be seen in the domain inside the cylinder. The data used for the test can be found in the title.

some numerical errors. The intensity plots can be seen in Figure 13, and the differences between the two solutions are found to be mainly quantitative.

So by looking at Figures 11 to 13 it can be seen that the numerical solution has some irregularities around the boundary of the cylinder due to the characteristic of the Hankel functions for small arguments. But since only the values on the boundary of the cylinder, which was seen in Figure 11, will be used in the final calculations, the numerical solution is found to be a good approximation of the exact solution. The method will be developed further to include two cylinders, and later also a Gaussian beam.

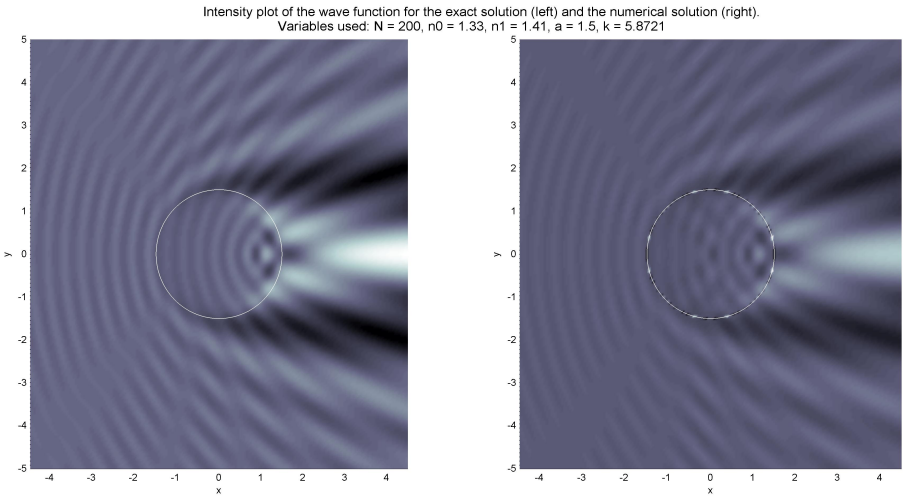

Figure 13: The exact solution for the wave function (left) is here compared with the numerical approximation of the boundary integral method (right), by intensity plots. The numerical solution has some irregularities on the boundary of the cylinder due to the characteristics of the Hankel functions. Except from this, the two solutions coincide with each other quite well. The data used for the test can be found in the title.

6 Two Cylinders

In the previous chapter a numerical solution for one cylinder placed in a host medium, was computed. The solution was found to be close to the exact solution found in Chapter 4. The numerical solution will now be extended to include two cylinders. As for the setup from the experiment reviewed in Chapter 2, the two cylinders will be placed on the x-axis, symmetrical around the y-axis. The first part of this chapter will derive the boundary integral equation for two cylinders, and then the solution for the whole domain will be calculated. In the end of the chapter the solution will be validated by comparing it with the exact solution for one cylinder.

6.1 The boundary integral equation for two cylinders

With two cylinders in the system, the influence between the cylinders needs to be taken into account, in addition to the influence from the plane wave. The equations for the wave function φ for this problem, will be similar to the equations for the problem with only one cylinder, but the influence between the cylinders will add a new term to these equations.

6.1.1 The wave function on the boundaries

For the problem with one cylinder, the equations for $\varphi(\zeta)$ on the boundary of the cylinder were found in Section 5.2, Equations 5.52 and 5.53 to be

$$\frac{1}{2}\varphi(\zeta) = \varphi_i(\zeta) - \int_{\partial\Omega}\Big(\varphi(\mathbf{x})\partial_{\mathbf{n}}G_0(\mathbf{x},\zeta) - G_0(\mathbf{x},\zeta)\partial_{\mathbf{n}}\varphi(\mathbf{x})\Big)\,dS(\mathbf{x}) \quad (6.1)$$

$$\frac{1}{2}\varphi(\zeta) = \int_{\partial\Omega}\Big(\varphi(\mathbf{x})\partial_{\mathbf{n}}G_1(\mathbf{x},\zeta) - G_1(\mathbf{x},\zeta)\partial_{\mathbf{n}}\varphi(\mathbf{x})\Big)\,dS(\mathbf{x}) \quad (6.2)$$

Where ζ, $\mathbf{x} \in \partial\Omega$. For a system with two cylinders there are two boundaries, so $\partial\Omega_j$ with $j = 1, 2$ denotes the boundary of cylinder one and cylinder two respectively. In addition, Ω_1 and Ω_2 denote the domain inside the two cylinders, while $\Omega_0 = (\Omega_1 + \Omega_2)^c$ denotes the domain outside the two cylinders, i.e. the host medium.

The two cylinders will affect each other as mentioned, but this only relates to the equation for the outer field Ω_0. Hence Equation 6.1 for the outer domain, will have an additional term involving the influence from a second cylinder. This new term will be similar to the boundary integral that is already there, but for the new term the integration will be over the other cylinder. Equation 6.2 for the domain inside a cylinder, will be the same as before, only the subscript numbers will change. So, for the problem with two cylinders, the equations for $\varphi(\zeta)$ with $\zeta \in \partial\Omega_1$, which is the boundary of cylinder one, are given as

$$\begin{aligned}\frac{1}{2}\varphi_1(\zeta) &= \varphi_i^1(\zeta) - \oint_{\partial\Omega_1}\left[\varphi_1(\mathbf{x})\partial_{\mathbf{n}}G_0(\mathbf{x},\zeta) - G_0(\mathbf{x},\zeta)\partial_{\mathbf{n}}\varphi_1(\mathbf{x})\right]\,dS(\mathbf{x}) \\ &\quad - \oint_{\partial\Omega_2}\left[\varphi_2(\mathbf{x})\partial_{\mathbf{n}}G_0(\mathbf{x},\zeta) - G_0(\mathbf{x},\zeta)\partial_{\mathbf{n}}\varphi_2(\mathbf{x})\right]\,dS(\mathbf{x}) \quad (6.3)\\ \frac{1}{2}\varphi_1(\zeta) &= \oint_{\partial\Omega_1}\left[\varphi_1(\mathbf{x})\partial_{\mathbf{n}}G_1(\mathbf{x},\zeta) - G_1(\mathbf{x},\zeta)\partial_{\mathbf{n}}\varphi_1(\mathbf{x})\right]\,dS(\mathbf{x}) \quad (6.4)\end{aligned}$$

And the equations for $\varphi(\zeta)$ with $\zeta \in \partial\Omega_2$, which is the boundary of cylinder two, are given as

$$\begin{aligned}\frac{1}{2}\varphi_2(\zeta) &= \varphi_i^2(\zeta) - \oint_{\partial\Omega_1}\left[\varphi_1(\mathbf{x})\partial_{\mathbf{n}}G_0(\mathbf{x},\zeta) - G_0(\mathbf{x},\zeta)\partial_{\mathbf{n}}\varphi_1(\mathbf{x})\right]\,dS(\mathbf{x}) \\ &\quad - \oint_{\partial\Omega_2}\left[\varphi_2(\mathbf{x})\partial_{\mathbf{n}}G_0(\mathbf{x},\zeta) - G_0(\mathbf{x},\zeta)\partial_{\mathbf{n}}\varphi_2(\mathbf{x})\right]\,dS(\mathbf{x}) \quad (6.5)\\ \frac{1}{2}\varphi_2(\zeta) &= \oint_{\partial\Omega_2}\left[\varphi_2(\mathbf{x})\partial_{\mathbf{n}}G_2(\mathbf{x},\zeta) - G_2(\mathbf{x},\zeta)\partial_{\mathbf{n}}\varphi_2(\mathbf{x})\right]\,dS(\mathbf{x}) \quad (6.6)\end{aligned}$$

Here G_j with $j = 0, 1, 2$, represents the Green's function in the host medium, cylinder one and cylinder two respectively, and φ_j represents the wave function on boundary j. Note that the Green's function and its normal derivative with subscript zero, G_0 and $\partial_{\mathbf{n}}G_0$, are different in all the four integral terms

where they arise. The subscript just shows that the function is calculated for the outer domain where the refraction index is n_0, but the values of $\mathbf{x}$ and ζ are different. More about this in Section 6.2 where the numerical computation and the results are discussed.

6.1.2 The wave function for the whole domain

In the same way as for the problem with one cylinder studied in Chapter 5, the domain solution for the problem with two cylinders can be found easily by applying the boundary integral method [6]. The equations for the wave function $\varphi(\zeta)$ in a given domain with only one cylinder present, were found in Section 5.3 on page 31 to be

$$\varphi(\zeta) = \varphi_i(\zeta) - \oint_{\partial\Omega} (\varphi(\mathbf{x})\partial_{\mathbf{n}}G_0(\mathbf{x},\zeta) - G_0(\mathbf{x},\zeta)\partial_{\mathbf{n}}\varphi(\mathbf{x}))\, dS(\mathbf{x}), \quad \zeta \in \Omega^c \tag{6.7}$$

$$\varphi(\zeta) = \oint_{\partial\Omega} (\varphi(\mathbf{x})\partial_{\mathbf{n}}G_1(\mathbf{x},\zeta) - G_1(\mathbf{x},\zeta)\partial_{\mathbf{n}}\varphi(\mathbf{x}))\, dS, \quad \zeta \in \Omega \tag{6.8}$$

For the case with two cylinders, the equations for the wave function in the outer domain, will have the same additional terms as the equations for the boundary solution, see Equations 6.3 and 6.5. The new terms represent the influence from the second cylinder. Hence, for the situation where two cylinders are placed in a host medium, the wave function $\varphi(\zeta)$ for the whole domain is found by the following equations:

$$\begin{aligned}\varphi(\zeta) = \varphi_i(\zeta) &- \oint_{\partial\Omega_1} (\varphi_1(\mathbf{x})\partial_{\mathbf{n}}G_0(\mathbf{x},\zeta) - G_0(\mathbf{x},\zeta)\partial_{\mathbf{n}}\varphi_1(\mathbf{x}))\, dS(\mathbf{x}) \\ &- \oint_{\partial\Omega_2} (\varphi_2(\mathbf{x})\partial_{\mathbf{n}}G_0(\mathbf{x},\zeta) - G_0(\mathbf{x},\zeta)\partial_{\mathbf{n}}\varphi_2(\mathbf{x}))\, dS(\mathbf{x}), \quad \zeta \in \Omega_0 \end{aligned} \tag{6.9}$$

$$\varphi(\zeta) = \oint_{\partial\Omega_1} (\varphi_1(\mathbf{x})\partial_{\mathbf{n}}G_1(\mathbf{x},\zeta) - G_1(\mathbf{x},\zeta)\partial_{\mathbf{n}}\varphi_1(\mathbf{x}))\, dS(\mathbf{x}), \quad \zeta \in \Omega_1 \tag{6.10}$$

$$\varphi(\zeta) = \oint_{\partial\Omega_2} (\varphi_2(\mathbf{x})\partial_{\mathbf{n}}G_2(\mathbf{x},\zeta) - G_2(\mathbf{x},\zeta)\partial_{\mathbf{n}}\varphi_2(\mathbf{x}))\, dS(\mathbf{x}), \quad \zeta \in \Omega_2 \tag{6.11}$$

The unknowns $\varphi_j(\mathbf{x})$ and $\partial_{\mathbf{n}}\varphi_j(\mathbf{x})$ on the right hand side of these equations were just found, so the wave function can easily be calculated for all values of ζ. The calculations for the wave field $\varphi(\zeta)$ with two cylinders present, will as all the previous calculations be performed in *Matlab*.

6.2 Numerical algorithm

The calculation of the wave function for two cylinders has been performed by numerical approximations in *Matlab*. First, a program calculates the values for φ_j and $\partial_{\mathbf{n}}\varphi_j$ on the boundaries of the two cylinders. Then these values will be used further to calculate the wave function for a given domain.

A short explanation of the procedures performed in the numerical approach will be given next, but the code in its entirety, together with a more detailed explanation can be found in Appendix C.

The program made in *Matlab* to perform the calculations for two cylinders, is similar to the program made for one cylinder, which was discussed in Section 5.4. The equation for this problem was given as $\mathbf{MX} = \mathbf{b}$. For the problem with two cylinders the same equation will be used, only now the block matrix $\mathbf{M}$ will be larger, consisting of more blocks than for the problem with one cylinder. The two vectors, $\mathbf{X}$ and $\mathbf{b}$, will also be larger due to the increased number of unknowns.

Matrix $\mathbf{M}$ is based on Equations 6.3 to 6.6. Notice that the Green's function and its normal derivative with index zero, G_0 and $\partial_{\mathbf{n}} G_0$, are different depending on the boundary for which the unknowns $\varphi_j(\mathbf{x})$ and $\partial_{\mathbf{n}}\varphi_j(\mathbf{x})$ are to be found. The Green's function and its derivative are functions of ζ and $\mathbf{x}$, where ζ will be on the boundary on the cylinder where the values are sought, and $\mathbf{x}$ will follow the integration path, which can be each of the two boundaries. Hence, when calculating the values on the boundary of cylinder one, G_0 and $\partial_{\mathbf{n}} G_0$ will be denoted as G_{11} and $\partial_{\mathbf{n}} G_{11}$ when the integration is over $\partial\Omega_1$, and G_{12} and $\partial_{\mathbf{n}} G_{12}$ for the integration over $\partial\Omega_2$. And equivalent for the calculation of the values on the boundary of the second cylinder, G_0 and $\partial_{\mathbf{n}} G_0$ will be denoted as G_{21} and $\partial_{\mathbf{n}} G_{21}$ when the integration is over $\partial\Omega_1$, and G_{22} and $\partial_{\mathbf{n}} G_{22}$ for the integration over $\partial\Omega_2$. All in all, this gives the following block matrix:

$$\mathbf{M} = \begin{pmatrix} \partial_{\mathbf{n}} G_1 & G_1 & \mathbf{0} & \mathbf{0} \\ \mathbf{0} & \mathbf{0} & \partial_{\mathbf{n}} G_2 & G_2 \\ \partial_{\mathbf{n}} G_{11} & G_{11} & \partial_{\mathbf{n}} G_{12} & G_{12} \\ \partial_{\mathbf{n}} G_{21} & G_{21} & \partial_{\mathbf{n}} G_{22} & G_{22} \end{pmatrix} \tag{6.12}$$

Then there is vector $\mathbf{b}$, which contains the incident wave vectors from Equations 6.3 and 6.5. The vectors φ_i^1 and φ_i^2 contain the values of the incident wave for each point on the boundaries of the two cylinders, and together they fill up half of vector $\mathbf{b}$. The other half of the vector contains just zeros since the other two Equations 6.4 and 6.6, do not add any terms to the right hand side of the matrix equation. From this, $\mathbf{b}$ is written as: $[\mathbf{0}\ \mathbf{0}\ \varphi_i^1\ \varphi_i^2]^T$.

The last vector, $\mathbf{X}$, contains the unknown values of $\varphi_j(\mathbf{x})$ and $\partial_{\mathbf{n}}\varphi_j(\mathbf{x})$ on the two boundaries, so $\mathbf{X} = [\varphi_1(\mathbf{x})\ \partial_{\mathbf{n}}\varphi_1(\mathbf{x})\ \varphi_2(\mathbf{x})\ \partial_{\mathbf{n}}\varphi_2(\mathbf{x})]^T$.

As for the problem with one cylinder, the matrix equation is solved in *Matlab* using Gaussian elimination: $\mathbf{X} = \mathbf{M}\backslash\mathbf{b}$. The unknown values on the two boundaries are then retrieved from vector $\mathbf{X}$.

Now having found the unknown values for the wave function and its normal derivative on the boundaries of the two cylinders, the boundary integral method makes it easy to calculate the wave function for the whole domain.

$\varphi(\zeta)$ is calculated from Equations 6.9 to 6.11, which give the following vector products for the wave function in the different domains.

$$\varphi(\zeta) = \begin{bmatrix} \partial_{\mathbf{n}} G_1 \\ G_1 \\ \mathbf{0} \\ \mathbf{0} \end{bmatrix} \cdot \begin{bmatrix} \varphi_1 \\ \partial_{\mathbf{n}} \varphi_1 \\ \varphi_2 \\ \partial_{\mathbf{n}} \varphi_2 \end{bmatrix}, \quad \zeta \in \Omega_1 \tag{6.13}$$

$$\varphi(\zeta) = \begin{bmatrix} \mathbf{0} \\ \mathbf{0} \\ \partial_{\mathbf{n}} G_2 \\ G_2 \end{bmatrix} \cdot \begin{bmatrix} \varphi_1 \\ \partial_{\mathbf{n}} \varphi_1 \\ \varphi_2 \\ \partial_{\mathbf{n}} \varphi_2 \end{bmatrix}, \quad \zeta \in \Omega_2 \tag{6.14}$$

$$\begin{aligned} \varphi(\zeta) = \varphi_i(\zeta) &- \begin{bmatrix} \partial_{\mathbf{n}} G_{11} \\ G_{11} \\ \partial_{\mathbf{n}} G_{12} \\ G_{12} \end{bmatrix} \cdot \begin{bmatrix} \varphi_1 \\ \partial_{\mathbf{n}} \varphi_1 \\ \varphi_2 \\ \partial_{\mathbf{n}} \varphi_2 \end{bmatrix} \\ &- \begin{bmatrix} \partial_{\mathbf{n}} G_{21} \\ G_{21} \\ \partial_{\mathbf{n}} G_{22} \\ G_{22} \end{bmatrix} \cdot \begin{bmatrix} \varphi_1 \\ \partial_{\mathbf{n}} \varphi_1 \\ \varphi_2 \\ \partial_{\mathbf{n}} \varphi_2 \end{bmatrix}, \quad \zeta \in \Omega_0 \end{aligned} \tag{6.15}$$

A more detailed description of the programming procedures can be found in Appendix C.

6.3 Validating the solution

In this section the solution of the wave field from the problem with two cylinders, will be compared with the exact solution for one cylinder. Despite the fact that the result found in this chapter is based on a problem with two cylinders, it is possible to compare the result with the exact solution for one cylinder by doing some adjustments. One method is to set the refraction index of one of the cylinders equal to the index of the host medium. Then this cylinder should be "invisible" to the waves, and should not contribute anything to the result. Another method is to move one of the cylinders far away from the other one. In this case, the wave field around one cylinder should not be influenced by the other cylinder as long as the distance between them is large enough.

First the method with the refraction index will be tested. One cylinder is centered about the origin to get the same setup as for the exact solution found in Chapter 4. The other cylinder is placed on the right side of the first cylinder. It does not matter though where this second cylinder is placed, since it has the same refraction index as the surroundings, and hence should

be "invisible". Figure 14 shows the solution for two cylinders with the given setup, together with the exact solution for one cylinder that was found earlier in this paper. The boundaries of the cylinders are marked with circles. The

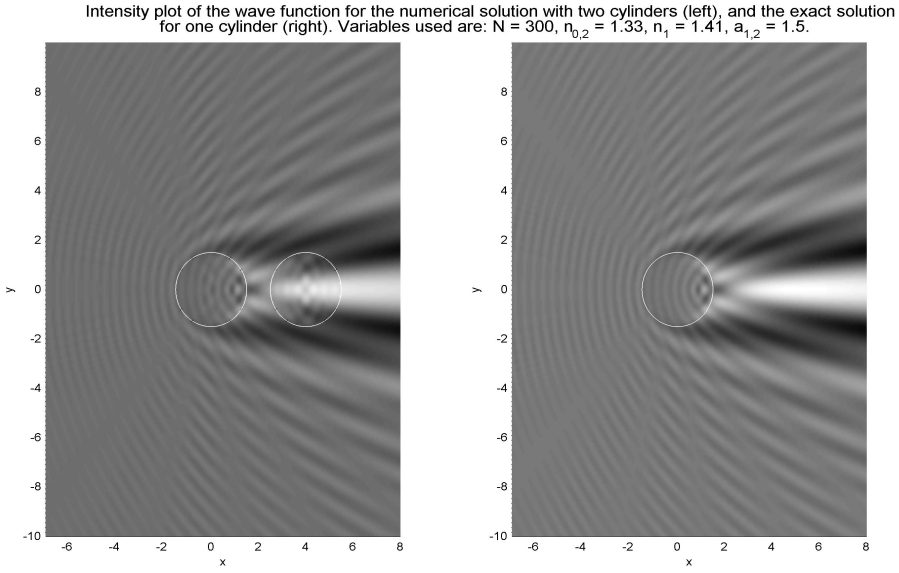

Figure 14: The numerical solution for the wave field for the problem with two cylinders is given in the left figure. Notice that the refraction index of the right cylinder has the same value as for the host medium, and hence it should not contribute anything to the wave field. But it can be seen in the figure that the field inside this cylinder is different from the corresponding domain in the figure on the right side. Hence, the domain is affected by the second cylinder to some extent. The values used in the calculation can be found in the title.

numerical solution has some irregularities on the boundaries of the cylinders due to the characteristic of the Hankel functions. In addition the field inside the second cylinder seems to be affected by the wave, even though the wave should not see this cylinder.

The wave field is also calculated along the x-axis for both the exact and the numerical solutions. The comparison between the two solutions along the x-axis can be seen in Figure 15. The irregularities on the boundaries of the two cylinders are easier to see in this plot. These irregularities arise due to the characteristic of the Hankel functions for small arguments. As for the intensity plot, the wave field for the numerical solution inside the second cylinder, which should be invisible, is different from the exact solution. Hence, except for the domain inside the second cylinder, the solution for the rest of the field seems to resemble the exact solution to a great extent. So all in all the numerical solution seems to be quite good.

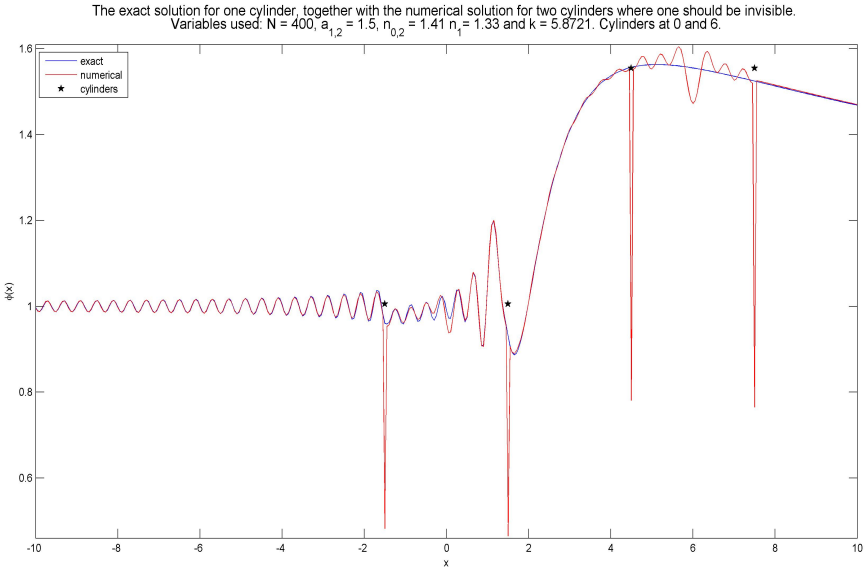

Figure 15: The exact solution for one cylinder is plotted together with the numerical solution for two cylinders. For the numerical solution the cylinder centered about $x = 6$ has the same refraction index as the surroundings, and hence it should be invisible and not affect the wave field. The figure shows that the cylinder is not completely invisible to the wave field. Both cylinders are marked with black stars in the plot.

The second method was to move one of the cylinders far away from the other one. Again, one cylinder is placed at the origin, while the other cylinder will be placed at a distance, a million times the radius of the first cylinder, away from the origin. For this method the two cylinders have the same refraction index, which is different from the index of the host medium. For the given distance, the two cylinders should not have any influence on each other. Figure 16 shows the solution for two cylinders, where one of them is too far away to make the picture, together with the exact solution for one cylinder. The two solutions resemble each other quite well, and it is hard to separate the exact solution from the numerical solution.

The numerical solution is also compared to the exact solution for the values of the wave function along the x-axis. In Figure 17 it can be seen that the two solutions resemble each other quite well, except for the values on the boundary, and also some small differences in the wave field inside the cylinder. The same could be seen in the intensity plot.

From these last few figures, the conclusion is that the numerical solution resembles the exact solution to a great extent. The only differences visible to the naked eye, are some irregularities on the boundaries of the cylinders,

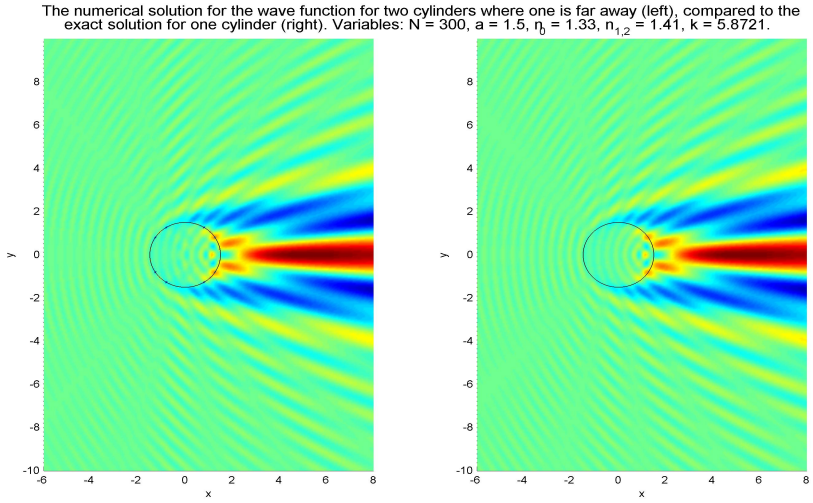

Figure 16: The left figure shows the numerical solution for the problem with two cylinders. The cylinders have the same refraction index, but the second cylinder is placed at a distance of 10^6 times the radius of cylinder one. At this distance the second cylinder should not influence on the field around the other cylinder, and the result should equal the exact solution for one cylinder seen in the right figure. The solutions seem to resemble each other quite well. The data used in the calculations can be found in the title.

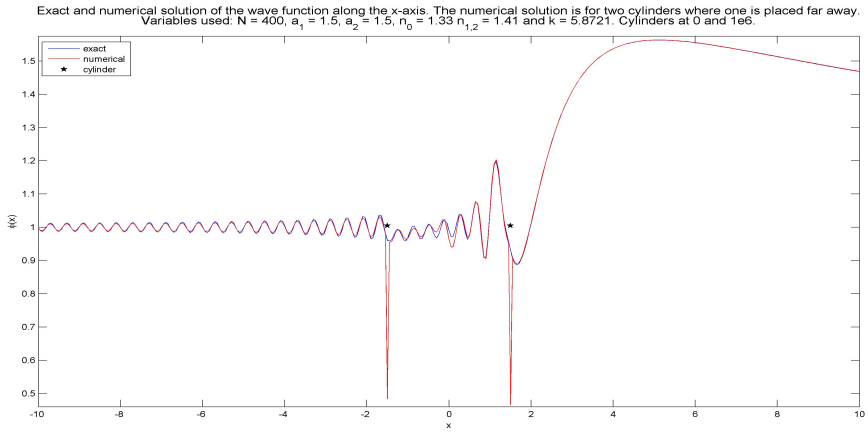

Figure 17: The exact solution for one cylinder along the x-axis, together with the numerical solution for two cylinders. The numerical problem includes two cylinders, but one is placed far away and hence the cylinders have no influence on each other. The stars mark the edges of the cylinder.

and also some small differences in the fields inside the cylinders. So the tests that have been performed to validate the numerical solution for two cylinders, show that both the numerical method and the boundary integral method makes a good approximation to the exact solution.

6.4 Wave field for two cylinders

The numerical solution of the problem with two cylinders has been compared with the exact solution, and is found to be a good approximation. The resulting wave field for two cylinders can be seen in Figure 18. Some of

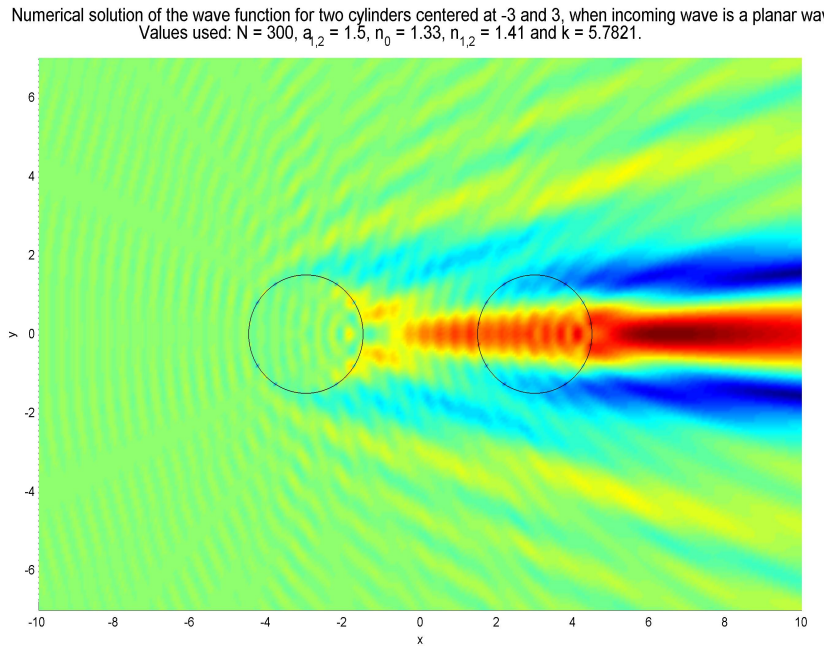

Figure 18: The resulting wave field for the problem with two cylinders placed symmetrical around the y-axis. A plane wave enters from the left, and the cylinders have the same refraction index, which is different than for the surroundings. The data from the calculations can be found in the title.

the boundary values stand out in the field, showing where the cylinders are situated. These values are due to some irregularities that will occur for small arguments in the calculations, which is the case near the boundaries. The same can be seen in Figure 19, where the solution of the wave function calculated along the x-axis. The irregularities on the boundaries of the cylinders are easier to see here.

The setup for the program is now approaching the setup for the experiment that was summarized in Chapter 2. Two cylinders are place symmetrical around the y-axis, and a planar wave enters from the left. The next

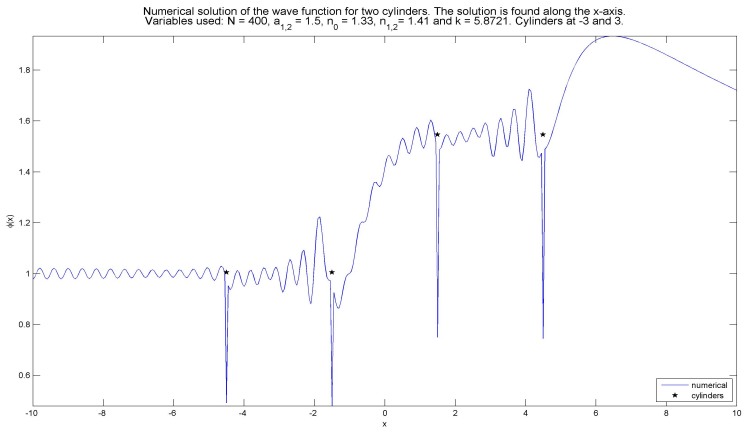

Figure 19: The solution of the wave function for the problem with two cylinders placed symmetrical around the y-axis. The solution is calculated along the x-axis, and some irregularities can be seen on the boundaries of the cylinders. The data used in the calculations can be found in the title.

step in the approach is to replace the plane wave with a Gaussian beam.

7 Gaussian Beam

A plane wave has been used as the incident wave in the calculations so far, but to approach the setup from the experiment this paper is based on, the plane wave will now be replaced with a two-dimensional Gaussian beam.

7.1 The Gaussian beam equation

In optics, and especially in laser optics, one often encounters Gaussian beams, which is a solution to the paraxial Helmholtz equation [1]. The power of the beam is mainly concentrated within a small cylinder surrounding the beam axis. The intensity distribution for any transverse plane, is a circularly symmetric Gaussian function centered about the beam axis. For instance, the transverse profile of the intensity of the beam with a power P can be described as a Gaussian function in the following way [24]:

$$I(r,z) = \frac{2P}{\pi W^2(z)} \exp\left(-2\frac{r^2}{W^2(z)}\right) \tag{7.1}$$

Here r is the distance from the center of the beam, and z is the distance from its waist. $W(z)$ is the beam radius defined as the distance from the beam axis (where the peak value of the beam intensity is assumed), to where the intensity drops to $1\backslash e^2$ of the maximum value. The function's width has its

minimum at the beam waist, W_0, and from here it grows gradually in both directions. The wavefronts are nearly planar near the waist of the beam, but they gradually curve and become approximately spherical far from the waist. Under ideal conditions, the light from a laser takes the form of a Gaussian beam [1]. A sketch of a Gaussian beam can be seen in Figure 20.

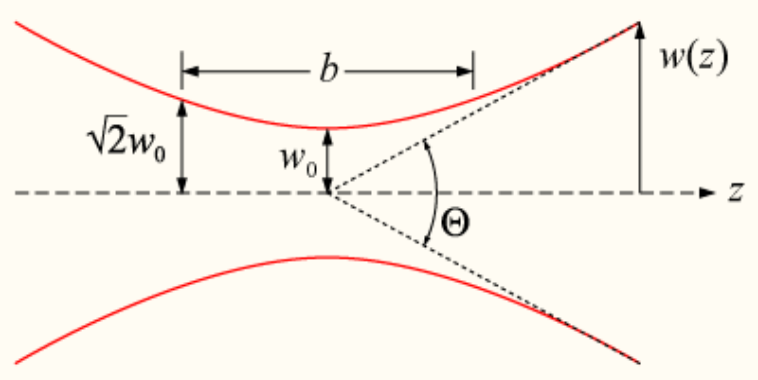

Figure 20: Diagram of Gaussian beam parameters. W_0 is the beam waist radius, *W(z)* is the beam radius, b is the confocal parameter of the beam and Θ is the total angular spread of the beam far from its waist [25].

This paper deals with a two dimensional problem, hence a two dimensional Gaussian beam will be used. The beam should propagate in the positive x-direction, and the focal point of the Gaussian beam will be located at $(-x_0, y_0)$.

The electric field is, as mentioned earlier in the paper, parallel to the cylinder axis (z-axis), and hence the electric field only has a z-component. The spatial distribution of the amplitudes E_z and E_y, in the plane located at $x = x_0$, can be given as [26]

$$E_z(-x_0, y, z) = E_0 \exp\left[-\frac{(y - y_0)^2}{W_0^2}\right] \tag{7.2}$$

$$E_y(-x_0, y, z) = 0 \tag{7.3}$$

Where W_0 is the beam waist radius. The field components in Cartesian coordinates can be expanded in an angular spectrum of plane waves [27]

$$E_x(x, y, z) = \int_{-\infty}^{\infty} A_x(p, q) \exp\left[ikn_0(px + qy)\right]\, dq \tag{7.4}$$

$$E_y(x, y, z) = \int_{-\infty}^{\infty} A_y(p, q) \exp\left[ikn_0(px + qy)\right]\, dq \tag{7.5}$$

$$E_z(x, y, z) = \int_{-\infty}^{\infty} A_z(p, q) \exp\left[ikn_0(px + qy)\right]\, dq \tag{7.6}$$

Where $p^2 + q^2 = 1$.

The complex amplitudes A_x, A_y and A_z are determined from the electric field components in the plane $x = -x_0$, and are given as

$$A_z(p,q) = \frac{1}{\lambda}\int_{-\infty}^{\infty} E_z(-x_0,y,z)\exp\left[-ikn_0(px+qy)\right]\,dy \tag{7.7}$$

$$= \frac{1}{\lambda}\int_{-\infty}^{\infty} E_0\exp\left[-\frac{(y-y_0)^2}{W_0^2}\right]\exp\left[-ikn_0(px+qy)\right]\,dy \tag{7.8}$$

$$= \frac{E_0\sqrt{\pi}W_0}{\lambda}\exp\left[-\frac{1}{4}k^2n_0^2W_0^2q^2\right]\exp(ikn_0pz_0 - ikn_0qy_0) \tag{7.9}$$

In a similar way $A_y(p,q)$ will be zero, since $E_y(x_0,y,z) = 0$, and also $A_x(p,q) = 0$ [26]. Hence

$$E_x(x,y,z) = 0, \qquad E_y(x,y,z) = 0 \tag{7.10}$$

And the equation for E_z is given as

$$E_z(x,y,z) = \frac{E_0\sqrt{\pi}W_0}{\lambda}\int_{-\infty}^{\infty}\exp\left[-\frac{1}{4}k^2n_0^2W_0^2q^2\right]\exp\Big(ikn_0[p(x+x_0)+q(y-y_0)]\Big)\,dq \tag{7.11}$$

Where E_z satisfies the Helmholtz equation

$$\left(\nabla^2 + k^2\right)E_z(x,y,z) = 0 \tag{7.12}$$

So the equation that will be used as the Gaussian beam in this paper is Equation 7.11. In the next section some comments are made about the numerical procedures, and in Section 7.3 the field for the Gaussian beam is compared with the field for the plane wave. Also, the result for the wave field with two cylinders and a Gaussian beam as the incident wave, can be found in this section.

7.2 Numerical implementation

The values for the Gaussian beam are found numerically in *Matlab* by a function that uses the built-in algorithm *quadl* to solve the integral in the equation for the beam. The algorithm approximates the integral, to within an error of 10^{-6}, using recursive adaptive Lobatto quadrature [23]. Except for this algorithm, the rest of the calculation of the Gaussian beam is straight forward. The code for the numerical implementation of the Gaussian beam can be view in Appendix C.

7.3 Comparison and results

The values for the incident wave φ_i, will now be calculated from the equation for the Gaussian beam (see Equation 7.11), instead of the plane wave

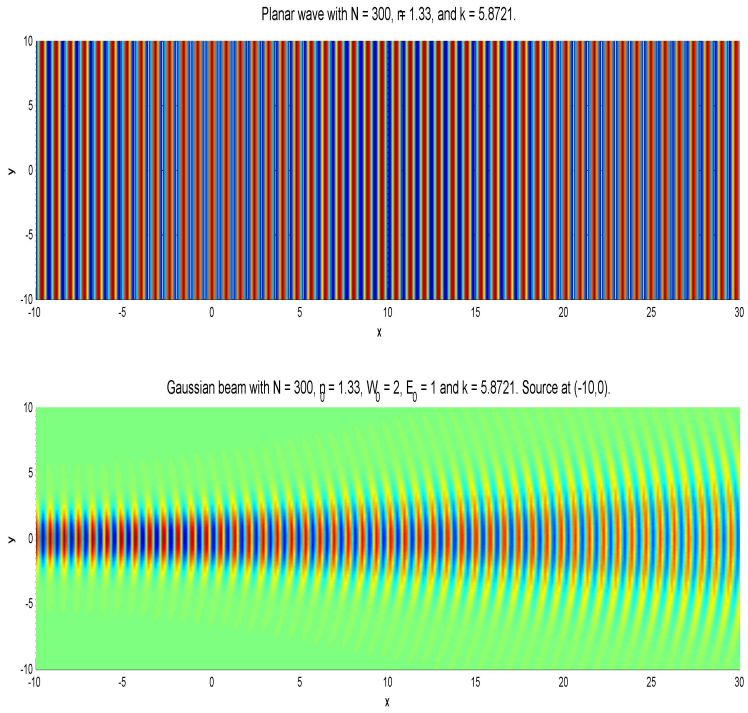

Figure 21: The figure at the top shows an intensity plot of a planar wave, while the bottom figure shows an intensity plot of a Gaussian beam. The Gaussian beam has a more narrow intensity field, and its wavefront goes from being almost planar in the beginning, to having a more spherical shape in the end. The data used in the calculations can be found in the titles.

equation used earlier in the paper. Figure 21 shows the difference in the intensity field of a Gaussian beam versus a plane wave. The differences between the two wave types are clear. The Gaussian beam has a more narrow intensity field, and the change of the wavefront shape, from nearly planar in the beginning to a more spherical shape in the end, can be seen in the figure.

The power of the beam is mainly concentrated within a small cylinder surrounding the beam axis. So by moving the source in the y-direction, away from the center of the cylinder, the intensity-field of the beam that hits the cylinder will be lower. This can be seen in Figure 22 where the source has been placed at two different y-values, while the cylinder stays at $y = 0$. The highest value is found when the source is placed at $y = 0$ as expected, since the intensity is highest at the beam axis.

In the rest of this paper, the Gaussian beam replaces the planar wave as the incident wave φ_i, in the calculations for the wave field. Figure 23

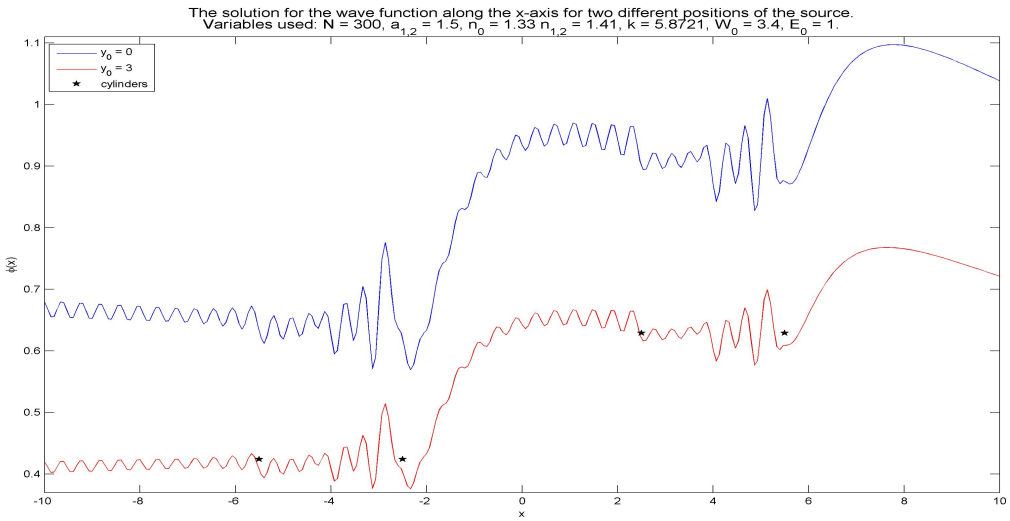

Figure 22: The value of the wave function along the x-axis for two different positions of the source. The source has been moved to a higher y value in the red graph, which gives a lower intensity on the field around the cylinder. The data used in the calculations can be found in the title.

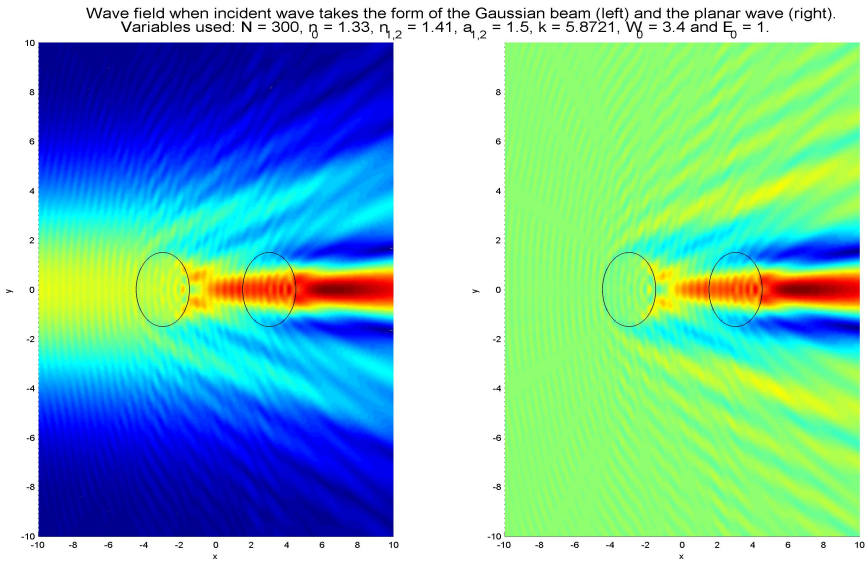

Figure 23: Solution of the wave field for two cylinders when the incident wave is a Gaussian beam (left figure), and when the incident wave takes the form of a plane wave (right figure). The cylinders are here placed at $(\mp 3, 0)$. The rest of the data used in the calculation is given in the title.

shows the result for the wave field, with the Gaussian beam as the incident wave. The figure also shows the result when the incident wave is a plane wave, just to see the difference between the two. The cylindrical shape of the Gaussian intensity field around the x-axis is easy to see in the figure. Other than that, the intensity field behind the cylinders resembles for the two wave types. However, this does not mean that they have the same values here, just that they have the same intensity distribution in that area.

The Gaussian beam has now been embodied into the program for calculating the wave field, so the program should resemble the setup from the experiment summarized in Chapter 2 quite good. Hence, the calculations of the forces acting on the two cylinders can be performed. But first the next chapter will go through some scaling of the equations that are used.

8 Scaling Laws

The problem in this paper is a small scale problem, and the diameter of the cylinders is in the size of micrometers. Scaling laws give the opportunity to scale this up to a larger scale problem that might be easier to work with, for instance for an experiment. In the following chapter some scaling laws will be given, and a scaling parameter for the forces that are sought will be found.

8.1 Scaling Maxwell's equations

Maxwell's equations for a source free dielectricum were found in the beginning of Chapter 4 to be

$$\begin{aligned} \nabla \times \mathbf{E} + \partial_t \mathbf{B} &= 0 && (8.1)\\ \nabla \times \mathbf{B} - \mu_0 \varepsilon_0 n^2(\mathbf{x}) \partial_t \mathbf{E} &= 0 && (8.2)\\ \nabla \cdot \mathbf{B} &= 0 && (8.3)\\ \nabla \cdot (n^2(\mathbf{x})\mathbf{E}) &= 0 && (8.4) \end{aligned}$$

Here the constitutive equations found on page 10,

$$\begin{aligned} \mathbf{B}(\mathbf{x}) &= \mu_0 \mathbf{H}(\mathbf{x}) && (8.5)\\ \mathbf{D}(\mathbf{x}) &= \varepsilon_0 n(\mathbf{x}) \mathbf{E}(\mathbf{x}) && (8.6) \end{aligned}$$

have been used to replace the **H**- and **D**-fields in Maxwell's equations from Chapter 4, with the **B**- and **E**-fields respectively. The rest of the parameters are as before the refraction index n, the magnetic permeability μ_0, and the electric permittivity ε_0.

The parameters in Maxwell's equations above, are then scaled as follows:

$$\mathbf{E} = E_0 \tilde{\mathbf{E}}, \quad \mathbf{B} = B_0 \tilde{\mathbf{B}}, \quad \mathbf{x} = L \tilde{\mathbf{x}}, \quad t = T \tilde{t} \qquad (8.7)$$

The marked parameters are dimensionless. Using these relations, the curl of a function is written as $\nabla_{\mathbf{x}}\times = \frac{1}{L}\tilde{\nabla}_{\tilde{\mathbf{x}}}\times$ and the time derivative is written as $\partial_t = \frac{1}{T}\partial_{\tilde{t}}$. Hence, the dimensionless Maxwell equations are given as

$$\tilde{\nabla}\times\tilde{\mathbf{E}} + \frac{LB_0}{TE_0}\,\partial_{\tilde{t}}\tilde{\mathbf{B}} = 0 \tag{8.8}$$

$$\tilde{\nabla}\times\tilde{\mathbf{B}} - \frac{LE_0}{TB_0}\mu_0\varepsilon_0 n^2(\tilde{\mathbf{x}})\,\partial_{\tilde{t}}\tilde{\mathbf{E}} = 0 \tag{8.9}$$

$$\tilde{\nabla}\cdot\tilde{\mathbf{B}} = 0 \tag{8.10}$$

$$\tilde{\nabla}\cdot(n^2(\tilde{\mathbf{x}})\tilde{\mathbf{E}}) = 0 \tag{8.11}$$

To get rid of the constant in front of the time derivative in the first of these four equations, a suitable scaling for $\mathbf{B}$, or B_0, is found to be

$$\frac{LB_0}{TE_0} = 1 \;\rightarrow\; B_0 = \frac{T}{L}E_0 \tag{8.12}$$

Replacing B_0 in Equation 8.9 with this expression, gives a new constant in front of the time derivative: $(\frac{L}{T})^2\mu_0\,\varepsilon_0\,n^2(\tilde{\mathbf{x}})$. Then $\mu_0\varepsilon_0$ is replaced with c^{-2}, where c is the speed of light, which gives $(\frac{L}{Tc})^2\,n^2(\tilde{\mathbf{x}})$. To get rid of the remaining constants, a length scale L is given, and the time-scale is chosen so that $\frac{L}{T} = c \rightarrow T = \frac{L}{c}$. Hence, only $n^2(\tilde{\mathbf{x}})$ remains in front of the time derivative. This simplifies Maxwell's equations further to give

$$\tilde{\nabla}\times\tilde{\mathbf{E}} + \partial_{\tilde{t}}\tilde{\mathbf{B}} = 0 \tag{8.13}$$

$$\tilde{\nabla}\times\tilde{\mathbf{B}} - n^2(\tilde{\mathbf{x}})\partial_{\tilde{t}}\tilde{\mathbf{E}} = 0 \tag{8.14}$$

$$\tilde{\nabla}\cdot\tilde{\mathbf{B}} = 0 \tag{8.15}$$

$$\tilde{\nabla}\cdot(n^2(\tilde{\mathbf{x}})\tilde{\mathbf{E}}) = 0 \tag{8.16}$$

There are now two free variables; E_0 and L. The latter one, L, used as the length scale, is fixed by setting it equal to the size of the scattering particles. In the problem at hand, the particles are in the size of microns, so $L = 1\,\mu m = 10^{-6}\,m$. The other free variable, E_0, will be calculated from the initial field from the laser beam. In experiments it is common to give the total energy flux from the initial field measured in watt. An expression for E_0 involving the total energy flux, P, will be derived in the following.

8.2 The total energy flux

The energy per unit time, per unit area, transported by the electromagnetic field is called the Poynting's vector, and is given as [12]

$$\mathbf{S} = \frac{1}{\mu_0}\mathbf{E}\times\mathbf{B} \tag{8.17}$$

The energy flux is then given as the energy per unit time crossing the infinitesimal surface $d\mathbf{a}$, that is $\mathbf{S}\cdot d\mathbf{a}$. Hence, the total energy flux P, through

a surface $\mathcal{S}$, is given as the surface integral over the average Poynting's vector [28]

$$P = \int_{\mathcal{S}} < \mathbf{S} > \cdot \mathbf{n}\, d\mathbf{a} \tag{8.18}$$

And the average Poynting's vector is given as

$$< \mathbf{S} > = \frac{1}{\tau} \int_0^\tau \mathbf{S}(t)\, dt, \quad \tau = \frac{2\pi}{\omega} \tag{8.19}$$

Where ω is the angular frequency.

For stationary fields, the electric field and the magnetic induction field can be written the following way

$$\mathbf{E}(\mathbf{x}, t) = \frac{1}{2} \left\{ \mathbf{E}(\mathbf{x}) e^{-i\omega t} + \mathbf{E}^*(\mathbf{x}) e^{i\omega t} \right\} \tag{8.20}$$

$$\mathbf{B}(\mathbf{x}, t) = \frac{1}{2} \left\{ \mathbf{B}(\mathbf{x}) e^{-i\omega t} + \mathbf{B}^*(\mathbf{x}) e^{i\omega t} \right\} \tag{8.21}$$

From these stationary fields, the average Poynting's vector is found to be

$$\begin{aligned} < \mathbf{S} > &= \frac{1}{\tau} \int_0^\tau \frac{1}{4\mu_0} [\mathbf{E} \times \mathbf{B} e^{-2i\omega t} + \mathbf{E}^* \times \mathbf{B} + \mathbf{E} \times \mathbf{B}^* + \mathbf{E}^* \times \mathbf{B}^* e^{2i\omega t}]\, dt \\ &= \frac{1}{2\mu_0} Re \left\{ \mathbf{E} \times \mathbf{B}^* \right\} \end{aligned} \tag{8.22}$$

Hence, the total energy flux given in Equation 8.18 is rewritten as

$$P = \frac{1}{2\mu_0} \int_{\mathcal{S}} Re \left\{ \mathbf{E} \times \mathbf{B}^* \right\} \cdot \mathbf{n}\, dS \tag{8.23}$$

To find the value for this total energy flux, the **E**- and **B**-fields must be calculated. This will be done in the next section.

8.3 The electric field and the magnetic induction field

The electric field only has a z-component as mentioned earlier in the paper, so the field can be written as

$$\mathbf{E} = \varphi(x, y) e_z \tag{8.24}$$

Here φ is a wave function, which solves the two dimensional Helmholtz equation $(\nabla^2 + k^2 n_j^2)\varphi = 0$. The corresponding **B**-field is found from the Maxwell equation $\nabla \times \mathbf{E} = i\omega \mathbf{B}$ found in Section 4.1 on page 10, which gives

$$\begin{aligned} \mathbf{B} &= \frac{1}{i\omega} \nabla \times \mathbf{E} \\ &= \frac{1}{i\omega} (\partial_y \varphi\, e_x, -\partial_x \varphi\, e_y) \end{aligned} \tag{8.25}$$

For the scattering field from a cylinder, it is assumed that the source produces a wave of the same type, which means that the incident wave can be written as $\varphi_i(x,y)e_z$. The source is a model of a laser beam, and must be a solution to the Helmholtz equation. This holds for the Gaussian beam that was found in Chapter 7 on page 46 and given as

$$E_z(x,y,z) = \frac{E_0\sqrt{\pi}W_0}{\lambda}\int_{-\infty}^{\infty}\exp\left[-\frac{1}{4}k^2n_0^2W_0^2q^2\right]\exp\Big(ikn_0[p(x+x_0)+q(y-y_0)]\Big)\,dq \tag{8.26}$$

Assuming that the transverse profile of the wave is gaussian for $x = -x_0$, the incident wave takes the following form

$$\mathbf{E}_i = \varphi_i(-x_0,y) = E_0e^{-y^2/W_0^2} \tag{8.27}$$

Where W_0 is the beam waist radius. So now, expressions for the electric field $\mathbf{E}$, and the magnetic induction field $\mathbf{B}$, are found and will be used for calculating the Gaussian beam amplitude E_0 from the total energy flux P.

8.4 Gaussian beam amplitude

Having found the electric field $\mathbf{E}$, the magnetic induction field $\mathbf{B}$ can be calculated from Equation 8.25, and then the total energy flux is calculated from the expression found in Equation 8.23. The normal vector in this equation points in the direction of the wave propagation, so the normal vector can be replaced with e_x. This, together with the expressions for the $\mathbf{E}$- and $\mathbf{B}$-fields, give the following calculation for the total energy flux:

$$\begin{aligned}
P &= \frac{1}{2\mu_0}\int_{\mathcal{S}} Re\,\{\mathbf{E}\times\mathbf{B}^*\}\cdot\mathbf{n}\,dS \\
&= \frac{1}{2\mu_0}\int_{-\infty}^{\infty} Re\left\{\varphi\frac{i}{\omega}\partial_x\varphi^*e_x + \varphi\frac{i}{\omega}\partial_y\varphi^*e_y\right\}\cdot e_x\,dy \\
&= \frac{1}{2\mu_0}\int_{-\infty}^{\infty} Re\left\{\varphi\frac{i}{\omega}(-ikn_0)\varphi^*e_x\right\}\cdot e_x\,dy \\
&= \frac{1}{2\mu_0}\int_{-\infty}^{\infty}\frac{kn_0}{\omega}\varphi\varphi^*\,dy
\end{aligned} \tag{8.28}$$

Where $\partial_x\varphi$ is found from Equation 8.26. The integration is over an infinitely strip, so that the computed total energy flux P, is computed in power per unit length.

The simplified expression for the Gaussian beam found in Equation 8.27 is put into the equation for P above, which gives

$$\begin{aligned} P &= \frac{1}{2\mu_0} \int_{-\infty}^{\infty} \frac{kn_0}{\omega} |E_0|^2 \, e^{-2y^2/W_0^2} \, dy \\ &= \frac{1}{2\mu_0} \frac{kn_0}{\omega} |E_0|^2 \int_{-\infty}^{\infty} e^{-2y^2/W_0^2} \, dy \\ &= \frac{1}{2\mu_0} \frac{kn_0}{\omega} |E_0|^2 \sqrt{\frac{\pi W_0^2}{2}} \end{aligned} \tag{8.29}$$

Hence the expression for E_0, the amplitude for the Gaussian beam, is found to be

$$|E_0| = \sqrt{\frac{P2\sqrt{2}\mu_0\omega}{\sqrt{\pi}W_0 k n_0}} \tag{8.30}$$

The total energy flux P is usually a known constant in an experiment. For the experiment that is the background for this paper, P was given as $100\,mW$. In this paper, P is computed in power per unit length along the z-axis of the cylinder. So by assuming that the power per length is the same as the total power (in three dimensions) used in the experiment, $P = 100\,mW$ will be used in the calculations here. Values for the magnetic permittivity μ_0, the angular frequency ω, the beam waist W_0 for the gaussian beam, the wavenumber k, and the refraction index n_0, are all given earlier in the paper.

In the next chapter the force on the two cylinders in the problem will be calculated, and the expression for E_0 that was just found, will be used to scale the force on the cylinders.

9 Forces on the Cylinders

Now when the wave solution is found, and the Gaussian beam has been introduced, the setup finally resembles the setup from the experiment this paper is based on. So the next step is to calculate the force on the two cylinders. In the experiment, the situation of interest was when the total force on the two cylinders was zero. In this paper a simplified setup with the problem in two dimensions, and with only one source is used, so the situation of interest is a little different compared to the experiment. Here, the situation where the force is the same on both cylinders is the one that is sought. In the end of the chapter, the result of the force calculation from the experiment in three dimensions, will be compared to the force calculation in two dimensions found here. The result will show if it is possible to model the three dimensional situation from the experiment, with the two dimensional situation covered in this thesis.

As mentioned in the introduction, due to the Minkowski form of the Energy-Momentum tensor for a material body, the force on a cylinder can be calculated just by knowing the wave field on the boundary of the cylinder [5]. From this, the total force on a cylinder is given as [12]

$$\mathbf{f} = \oint_{\mathcal{S}} \mathbf{T} \cdot d\mathbf{n} \tag{9.1}$$

Where $\mathbf{T}$ is Maxwell's stress tensor, the stress tensor of an electromagnetic field, on the boundary of a cylinder. So to find the total force, Maxwell's stress tensor needs to be calculated.

9.1 Maxwell's stress tensor

The Maxwell stress tensor was given in Chapter 3 on page 6 to be

$$\mathbf{T} = \mathbf{ED} + \mathbf{HB} - \frac{1}{2}\mathbf{I}\left(\mathbf{E}\cdot\mathbf{D} + \mathbf{H}\cdot\mathbf{B}\right) \tag{9.2}$$

Elementwise it can be written as

$$T_{ij} = \varepsilon\left(E_iE_j - \frac{1}{2}\delta_{ij}(\mathbf{E}\cdot\mathbf{E})\right) + \frac{1}{\mu_0}\left(B_iB_j - \frac{1}{2}\delta_{ij}(\mathbf{B}\cdot\mathbf{B})\right) \tag{9.3}$$

The Kronecker delta, δ_{ij}, takes the value *one* if the indices are the same, and *zero* otherwise. Physically, the stress tensor can be seen as the force per unit area (or stress) acting on a surface [29].

9.2 Time-averaged force

The force on the cylinders is averaged over time, and the time-domain average of the force for a period $\tau = \frac{2\pi}{\omega}$, is found to be

$$\mathbf{f}_{av} = \oint_{\mathcal{S}} \left(\frac{1}{\tau}\int_0^{\tau} \mathbf{T}\, dt\right)\cdot\, \mathbf{n}\, dS = \oint_{\mathcal{S}} <\mathbf{T}>\cdot\mathbf{n}\, dS \tag{9.4}$$

Writing the electromagnetic fields with the time-dependency $e^{i\omega t}$ gives

$$\mathbf{E} = \left(\mathbf{E}_0e^{-i\omega t} + \mathbf{E}_0^*e^{i\omega t}\right) \tag{9.5}$$

$$\mathbf{B} = \frac{1}{\mu_0}\left(\mathbf{B}_0e^{-i\omega t} + \mathbf{B}_0^*e^{i\omega t}\right) \tag{9.6}$$

Using these expressions for the electromagnetic fields, the stress tensor found in Equation 9.2 can be written as

$$\begin{aligned}\mathbf{T} = {} & \varepsilon\left(\mathbf{E}_0e^{-i\omega t} + \mathbf{E}_0^*e^{i\omega t}\right)\left(\mathbf{E}_0e^{-i\omega t} + \mathbf{E}_0^*e^{i\omega t}\right) \\ & + \frac{1}{\mu_0}\left(\mathbf{B}_0e^{-i\omega t} + \mathbf{B}_0^*e^{i\omega t}\right)\left(\mathbf{B}_0e^{-i\omega t} + \mathbf{B}_0^*e^{i\omega t}\right) \\ & - \frac{1}{2}\mathbf{I}\Big[\varepsilon\left(\mathbf{E}_0e^{-i\omega t} + \mathbf{E}_0^*e^{i\omega t}\right)\cdot\left(\mathbf{E}_0e^{-i\omega t} + \mathbf{E}_0^*e^{i\omega t}\right) \\ & + \frac{1}{\mu_0}\left(\mathbf{B}_0e^{-i\omega t} + \mathbf{B}_0^*e^{i\omega t}\right)\cdot\left(\mathbf{B}_0e^{-i\omega t} + \mathbf{B}_0^*e^{i\omega t}\right)\Big]\end{aligned} \tag{9.7}$$

From this, the time averaged stress tensor is found to be

$$< \mathbf{T} > = \Big(\varepsilon_0 n_0^2(\mathbf{E}_0\mathbf{E}_0^*) + \frac{1}{\mu_0}(\mathbf{B}_0\mathbf{B}_0^*) - \frac{1}{2}\,\mathbf{I}\Big[\varepsilon_0 n_0^2(\mathbf{E}_0\cdot\mathbf{E}_0^*) + \frac{1}{\mu_0}(\mathbf{B}_0\cdot\mathbf{B}_0^*)\Big]\Big) \;+\; \text{c.c.}$$
$$= \frac{1}{\mu_0}\Big(\varepsilon_0\mu_0 n_0^2(\mathbf{E}_0\mathbf{E}_0^*) + (\mathbf{B}_0\mathbf{B}_0^*) - \frac{1}{2}\,\mathbf{I}\Big[\varepsilon_0\mu_0 n_0^2(\mathbf{E}_0\cdot\mathbf{E}_0^*) + (\mathbf{B}_0\cdot\mathbf{B}_0^*)\Big]\Big) \;+\; \text{c.c.}$$

Where $c.c$ denotes the complex conjugate. The scaling parameters found in Chapter 8 will now be introduced to this time average stress tensor. In Equation 8.12 on page 50, the norm of the magnetic induction B_0, is found to be $B_0 = \frac{T}{L}E_0 = \frac{1}{c}E_0$. And since $\varepsilon_0\mu_0 = c^{-2}$, the expression for $< \mathbf{T} >$ simplifies to

$$< \mathbf{T} >= \frac{B_0^2}{\mu_0}\tilde{\mathbf{T}}, \tag{9.8}$$

where $\tilde{\mathbf{T}}$ is given as

$$\tilde{\mathbf{T}} = \Big(n_0^2\,(\tilde{\mathbf{E}}_0\tilde{\mathbf{E}}_0^*) + (\tilde{\mathbf{B}}_0\tilde{\mathbf{B}}_0^*) - \frac{1}{2}\,\mathbf{I}\Big[n_0^2\,(\tilde{\mathbf{E}}_0\cdot\tilde{\mathbf{E}}_0^*) + (\tilde{\mathbf{B}}_0\cdot\tilde{\mathbf{B}}_0^*)\Big]\Big) \;+\; \text{c.c.} \tag{9.9}$$

So $\tilde{\mathbf{T}}$ is a nondimensional stress tensor. Using this tensor, the time average force is rewritten as

$$\mathbf{f}_{av} = \frac{B_0^2}{\mu_0}\oint_{\mathcal{S}} \tilde{\mathbf{T}}\cdot\mathbf{n}\,dS \tag{9.10}$$

Equations for the electric field $\mathbf{E}$ and the magnetic induction field $\mathbf{B}$, for the problem with two cylinders, will be derived in the next section.

9.3 The electromagnetic fields, E and B

Writing the electric field $\mathbf{E}$ and the magnetic induction field $\mathbf{B}$, in terms of the wave function φ, the following expressions were found in Section 8.3 on page 51:

$$\mathbf{E} = (0,\, 0,\, \varphi) \tag{9.11}$$
$$\mathbf{B} = \frac{1}{i\omega}(\varphi_y,\, -\varphi_x,\, 0) \tag{9.12}$$

To be able to calculate the average force from Equation 9.10, the partial derivatives $\partial_x\varphi$ and $\partial_y\varphi$ of the wave function, needs to be found. The wave function and its normal derivative have been calculated earlier in this paper. The partial derivatives $\partial_x\varphi$ and $\partial_y\varphi$, can be calculated from the normal derivative $\partial_{\mathbf{n}}\varphi$, and the tangential derivative $\partial_{\mathbf{t}}\varphi$. The tangential derivative is not known, but it can be calculated through central difference [20]. The tangential derivative for each point m, on the boundary of one of the cylinders, is given as

$$\partial_{\mathbf{t}}\varphi_m = \frac{\varphi_{m+1} - \varphi_{m-1}}{2a\Delta\theta} \tag{9.13}$$

Where a is the radius of the cylinder, $\Delta\theta$ is the angle grid-size, and φ_m is the value of the wave function in point m. So now both the tangential and the normal derivatives of the wave function are known, and $\partial_x\varphi$ and $\partial_y\varphi$ will be calculated next.

A directional derivative of a function, f, was given in Section 5.2 on page 25 as

$$\partial_{\mathbf{v}} f(\mathbf{x}) = \nabla f(\mathbf{x}) \cdot \mathbf{v} \tag{9.14}$$

Here the directional derivative is taken in the direction of $\mathbf{v}$. Using this formula, $\partial_x\varphi$ and $\partial_y\varphi$ can be written as

$$\begin{aligned} \partial_x\varphi &= \nabla\varphi \cdot e_x & (9.15)\\ \partial_y\varphi &= \nabla\varphi \cdot e_y & (9.16) \end{aligned}$$

The unit vectors, e_x and e_y, relates to the unit normal vector, $\mathbf{n}$, and the unit tangential vector, $\mathbf{t}$, in the following way:

$$\begin{aligned} e_x &= (e_x \cdot \mathbf{n})\,\mathbf{n} + (e_x \cdot \mathbf{t})\,\mathbf{t} & (9.17)\\ e_y &= (e_y \cdot \mathbf{n})\,\mathbf{n} + (e_y \cdot \mathbf{t})\,\mathbf{t} & (9.18) \end{aligned}$$

Hence the partial derivative $\partial_x\varphi$, can be written as

$$\begin{aligned} \partial_x\varphi &= \nabla\varphi \cdot \Big((e_x \cdot \mathbf{n})\,\mathbf{n} + (e_x \cdot \mathbf{t})\,\mathbf{t}\Big)\\ &= (e_x \cdot \mathbf{n})(\nabla\varphi \cdot \mathbf{n}) + (e_x \cdot \mathbf{t})(\nabla\varphi \cdot \mathbf{t})\\ &= (e_x \cdot \mathbf{n})\partial_{\mathbf{n}}\varphi + (e_x \cdot \mathbf{t})\partial_{\mathbf{t}}\varphi & (9.19) \end{aligned}$$

And the partial derivative $\partial_y\varphi$, similarly becomes

$$\begin{aligned} \partial_y\varphi &= \nabla\varphi \cdot \Big((e_y \cdot \mathbf{n})\,\mathbf{n} + (e_y \cdot \mathbf{t})\,\mathbf{t}\Big)\\ &= (e_y \cdot \mathbf{n})\partial_{\mathbf{n}}\varphi + (e_y \cdot \mathbf{t})\partial_{\mathbf{t}}\varphi & (9.20) \end{aligned}$$

So all the unknown values that were sought are found, and the **E**- and **B**-fields can be written in terms of the wave function and its derivatives:

$$\begin{aligned} \mathbf{E} &= \varphi\, e_z & (9.21)\\ \mathbf{B} &= \frac{1}{i\omega}\Big(\left[(e_x \cdot \mathbf{n})\partial_{\mathbf{n}}\varphi + (e_x \cdot \mathbf{t})\partial_{\mathbf{t}}\varphi\right] e_x\\ &\quad - \left[(e_x \cdot \mathbf{n})\partial_{\mathbf{n}}\varphi + (e_x \cdot \mathbf{t})\partial_{\mathbf{t}}\varphi\right] e_y\Big) & (9.22) \end{aligned}$$

These expressions will now be used to calculate the average Maxwell stress tensor and then to calculate the force on the cylinders.

9.4 Calculating the force

Now that the partial derivatives are known, $\tilde{\mathbf{T}}$ from the averaged Maxwell stress tensor can be written in terms of φ, $\partial_x\varphi$ and $\partial_y\varphi$, instead of $\mathbf{E}$ and $\mathbf{B}$. The expression for $\tilde{\mathbf{T}}$ is found in Equation 9.9, and in terms of vectors the equation can be rewritten as

$$\begin{aligned}\tilde{\mathbf{T}} &= n_0^2\left(\begin{bmatrix}0\\0\\\varphi\end{bmatrix}[0,\ 0,\ \varphi^*] - \frac{1}{2}\mathbf{I}\left(\begin{bmatrix}0\\0\\\varphi\end{bmatrix}\cdot\begin{bmatrix}0\\0\\\varphi^*\end{bmatrix}\right)\right) \\ &\quad + \frac{1}{\omega^2}\left(\begin{bmatrix}\varphi_y\\-\varphi_x\\0\end{bmatrix}\left[\varphi_y^*,\ -\varphi_x^*,\ 0\right] - \frac{1}{2}\mathbf{I}\left(\begin{bmatrix}\varphi_y\\-\varphi_x\\0\end{bmatrix}\cdot\begin{bmatrix}\varphi_y^*\\-\varphi_x^*\\0\end{bmatrix}\right)\right) + \text{ c.c.}\end{aligned} \tag{9.23}$$

Where the star, *, denotes the complex conjugate of a vector. The tensor gives a 3-by-3 matrix for each point on the boundary of each cylinder. Since the problem in this paper is in two dimensions, the tensor is reduced to a 2-by-2 matrix representing the x- and y-directions.

So now, having found $\tilde{\mathbf{T}}$, the force one each cylinder can be calculated. The boundaries of the cylinders are parametrized to give the following

$$\begin{aligned}\mathbf{f}_{av} &= \frac{B_0^2}{\mu_0}\oint_{\mathcal{S}}\tilde{\mathbf{T}}\cdot\mathbf{n}\,dS \\ &= \frac{\tilde{a}LB_0^2}{\mu_0}\int_0^{2\pi}\tilde{\mathbf{T}}\cdot\mathbf{n}\,d\theta \\ &\approx \frac{\tilde{a}LB_0^2}{\mu_0}\left\{\sum_{j=1}^{N}\int_{\alpha_j}^{\alpha_{j+1}}\tilde{\mathbf{T}}\cdot\mathbf{n}\,d\theta\right\}\end{aligned} \tag{9.24}$$

Where $\tilde{a}$ is the scaled radius, and L is the length scale.

The grid size on the boundary of the cylinders is small, with $\Delta\theta << 1$. Hence, the values of $\tilde{\mathbf{T}}\cdot\mathbf{n}$ are assumed to be constant over the interval $[\alpha_j, \alpha_{j+1}]$. Then the expression for the force can be rewritten as

$$\mathbf{f}_{av} = \frac{\tilde{a}\Delta\theta LB_0^2}{\mu_0}\left\{\sum_{j=1}^{N}(\tilde{\mathbf{T}}\cdot\mathbf{n})(\theta_j)\right\} \tag{9.25}$$

Where $(\tilde{\mathbf{T}}\cdot\mathbf{n})(\theta_j)$ is the dot product of the tensor and the normal vector in point θ_j.

All the calculations in this chapter has been performed in *Matlab*. The next section gives a short explanation to these procedures.

9.5 Numerical algorithm

The code for the numerical calculation of the force on the cylinders, can be found in its entirety in Appendix D. In the following a short summary for the procedures performed in *Matlab* will be given.

To find the force on a cylinder, first of all the values for the wave function φ, and its normal derivative $\partial_{\mathbf{n}}\varphi$, are calculated at each point on the boundary. These values were calculated in Chapter 5 for the problem with one cylinder, and in Chapter 6 for two cylinders. Having found these values, the tangential derivative for the wave function is calculated using central difference, as shown in Equation 9.13. The derivative is calculated pointwise around the boundary, using the value of the wave function φ.

Having both the tangential and the normal derivatives, the partial derivatives, $\partial_x\varphi$ and $\partial_y\varphi$, are calculated using Equations 9.19 and 9.20. The calculations are straightforward as long as the normal and the tangential derivatives are known. Next, the tensor $\tilde{\mathbf{T}}$ is calculated from the expression found in Equation 9.23. The tensor gives a 3×3 matrix for each point on the boundary, which is reduced to a 2×2 matrix since the problem is only in two dimensions. Then the stress tensor is multiplied by the normal vector at each point on the boundary, and the vectors that come out of this multiplication are summarized for each cylinder. This results in one force vector for each cylinder. Finally the average force is found by multiplying the force vector by $\frac{\tilde{a}\Delta\theta LB_0^2}{\mu_0}$ as given in Equation 9.25.

9.6 Results from the Force Calculation

So, having found the force on the two cylinders in the problem, it is time to compare the result with the result from the experiment. The *Matlab* program that was made for calculating the force on the cylinders, has been run with refraction indices and distances between the cylinders equivalent to the values that were used in the experiment. The calculations have been performed with 800 grid points on the boundary of each cylinder to get as good result as possible. Time, and memory size of the computer, were limiting the number of grid points that could be used. Figure 24 shows the force on the two cylinders vs the distance between them, for two different refraction indices in the host medium. The oscillations seen for the force on the cylinder closest to the source (cylinder 1), were also found by Karasek et al. [30]. The oscillations are probably caused by the interference of the field from a single incident beam that are scattered by both cylinders.

To be able to make a comparison between the result found in this paper and the result from the experiment, the force is calculated for the same distances and refraction indices that were used in the experiment. Figure 25 shows the result from the experiment (same as Figure 2 on page 5), together with the result found in this paper. The distances between the two cylinders

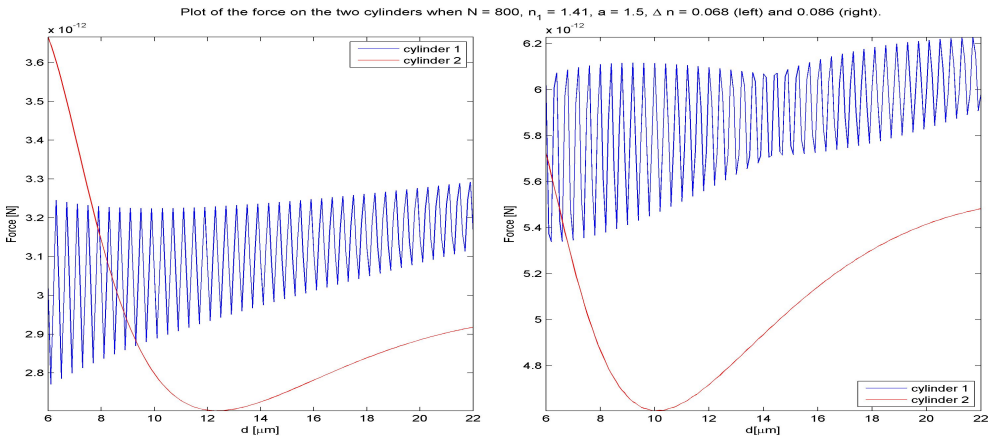

Figure 24: The force on the two cylinders for two different refraction indices. The force on the cylinder closes to the source (cylinder 1) have a noticeable oscillatory behavior, while the force on the second cylinder is a quite smooth graph.

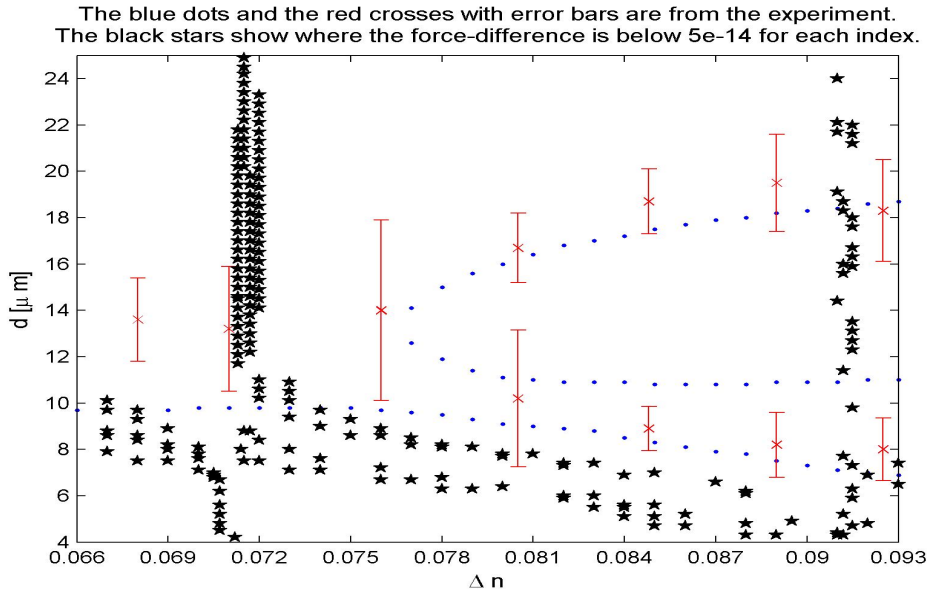

Figure 25: This figure without the stars, were shown in Chapter 2. It shows the result from the experiment with numerical data marked with blue dots, and the experimental results as red crosses with error bars. The black stars show where the values of the force difference, found by the numerical approximation in this paper, is below $5e^{-14}$.

that hold the three lowest values for the force difference, are marked as black stars for each refraction index. As mentioned earlier, the situation of interest in the experiment was when the total force on each cylinder were zero, while here the force on cylinder one should equal the force on cylinder two, in order to imitate the setup from the experiment with only one source. That is why the lowest values of the force difference and not the force is marked. Several stable configurations were also found by Karasek et al. [30], but they found stable configurations mostly inside the blue "half circle" for the upper half of the refraction index interval.

The potential for the force difference between the two cylinders is then calculated using the following relation

$$F = -\nabla V, \tag{9.26}$$

where V is the potential, and F is the force. The equation is solved using backward difference, and Figure 26 shows four examples of the potential for some different refraction indices.

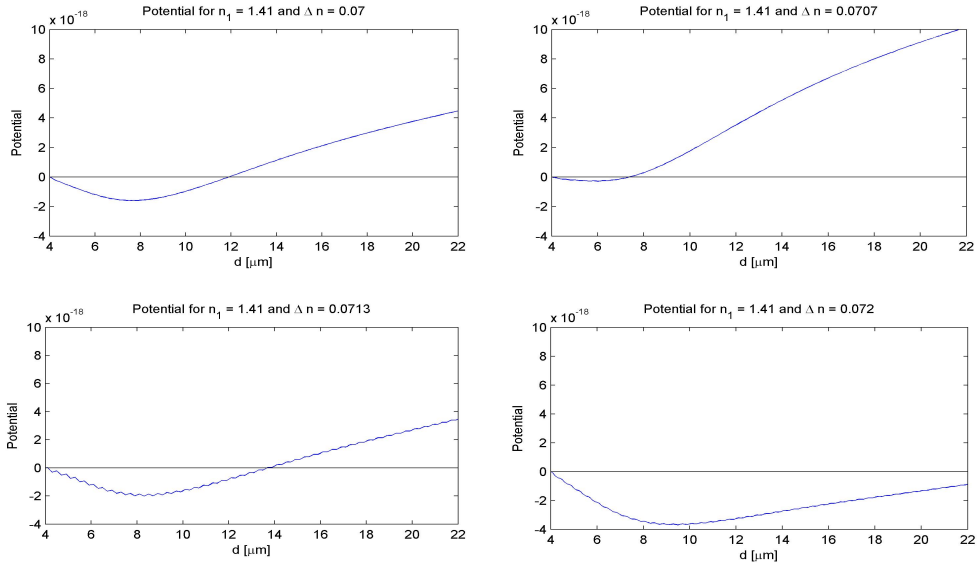

Figure 26: Potential for the force difference between the two cylinders for four different refraction indices.

In Figure 25, the result from the experiment was compared with the force difference that was found earlier in this chapter. The result from the experiment can also be compared with the minimum values of the potential for each refraction index. The distance between the cylinders that corresponds to the lowest potential is marked as black stars in Figure 27. It seems like the stars in this figure are approaching asymptotic values in two areas of the

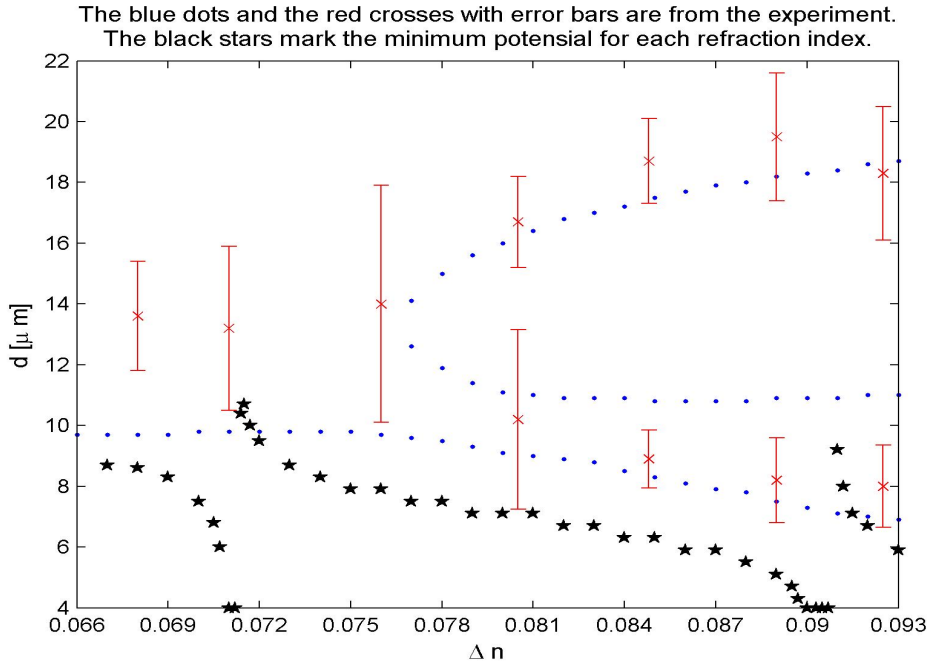

Figure 27: The minimum of the potential for each refraction index is marked in the figure. Notice the asymptotic behavior near $\Delta n = 0.071$ and $\Delta n = 0.090$.

refraction index interval. That is around $\Delta n = 0.071$ and $\Delta n = 0.090$. The same can be seen in Figure 25. Physically this means that if the cylinders are placed in a stable equilibrium, and then the refraction index of the host medium is changed to a value close to one of the values that were noticed in the figure, the cylinders would collide. For other refraction indices, the distance would change until equilibrium were found again, but for two areas in the refraction index interval there seem to be no equilibrium, hence the cylinders would collide. For some of the potential graphs that were shown in Figure 26 some oscillations could be seen. These oscillations are found for potentials around the Δn values mentioned above, and they show a region of several equilibrium configurations. The kinetic energy of the Brownian motion of the cylinders are found to be much lower than the work needed to move the cylinders from these equilibriums, which means that the positions are stable.

By examining all the results that are found in this section, there are evidently something happening around the refraction indices corresponding to $\Delta n = 0.071$ and $\Delta n = 0.090$. After doing some calculations and some testing of the data, the numerical values of the wave function on the boundary of the cylinders are found to be quite inaccurate for the refraction indices that

were just mentioned. The numerical calculation of the wave function on the boundary of a cylinder, was found to be quite good when it was examined in the end of Chapter 5, even for a relatively low number of grid points. See for instance Figure 11 on page 33. But it seems that for a few values of Δn, the numerical solution does not resemble the exact solution well enough. Figure 28 shows the numerical solution and the exact solution of the wave function on the boundary of a cylinder when $\Delta n = 0.0715$. The difference between

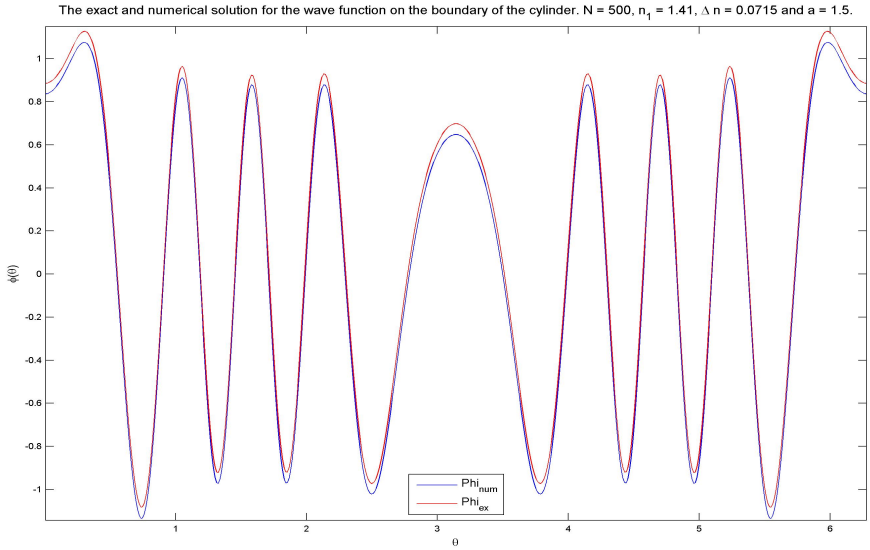

Figure 28: The numerical approximation of the wave solution on the boundary is not very good for $\Delta n = 0.0715$.

the two solutions is quite large, and far away from the accuracy that was found when the solutions were compared earlier in the paper, as mentioned above. There the difference between the exact solution and the numerical solution was not possible to see with the naked eye, while the difference in Figure 28 is quite substantial. For $\Delta n = 0.090$ the difference between the exact and numerical solutions is also found to be quite large. But except for some values of Δn that are close to the two mentioned values, the rest of the refraction indices give results that are in the same order of accuracy as what was found in Chapter 5.

It is not easy to say why the accuracy are so bad in these two areas. The values of the wave function on the boundary of the cylinders have been calculated from the integral equations that were found in Chapters 5 and 6. The integral equations are solved using a midpoint rule to make the numerical computations easier and faster. That is, instead of performing an integration, the midpoint in the interval multiplied by the width of the

interval was chosen as the value. This is not a very accurate way of solving the integral equations, but it was though of as a good enough approximation if the intervals on the boundary were small enough. The difference between solving the equations by integration, and by the midpoint rule, is found using the built-in function *quadl* in *Matlab* [23]. This function approximates an integral within an error of 1e-6. The integral equations for the wave function for $\Delta n = 0.0715$ is solved using *quadl*, and the result from this integration can be seen in Figure 29, where it is compared with the exact solution of the wave function, and the numerical solution that was found earlier in the paper. Clearly the midpoint approach is not good enough, while the result

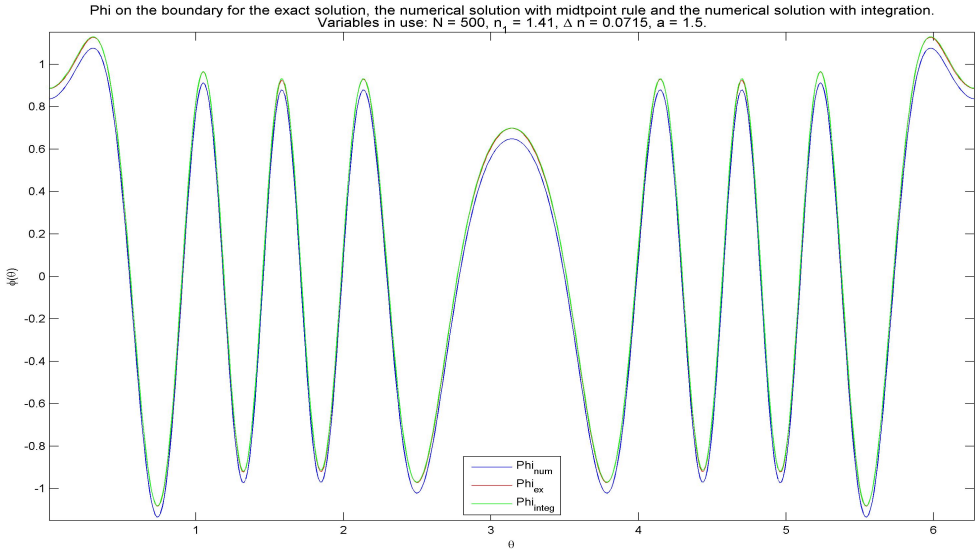

Figure 29: A better approximation of the wave function is found using the built-in function *quadl* in *Matlab*. The exact solution is almost covered by the solution found using the integration function *quadl*.

from *quadl* covers the exact solution quite good.

The way the integral equations have been solved using the midpoint rule, is definitely something that should have been improved, but since the problem with certain refraction indices was discovered so late in the process, there is not enough time to make the changes. At least the result for most of the refraction indices are found to be quite accurate. Figure 30 shows the wave function on the boundary of a cylinder for the three different approaches using another Δn. The figure shows the situation that is representative for most refraction indices, where the difference between using the *quadl* function and the midpoint rule is not that substantial. The right plot in the figure has been magnified quite a bit to be able to separate

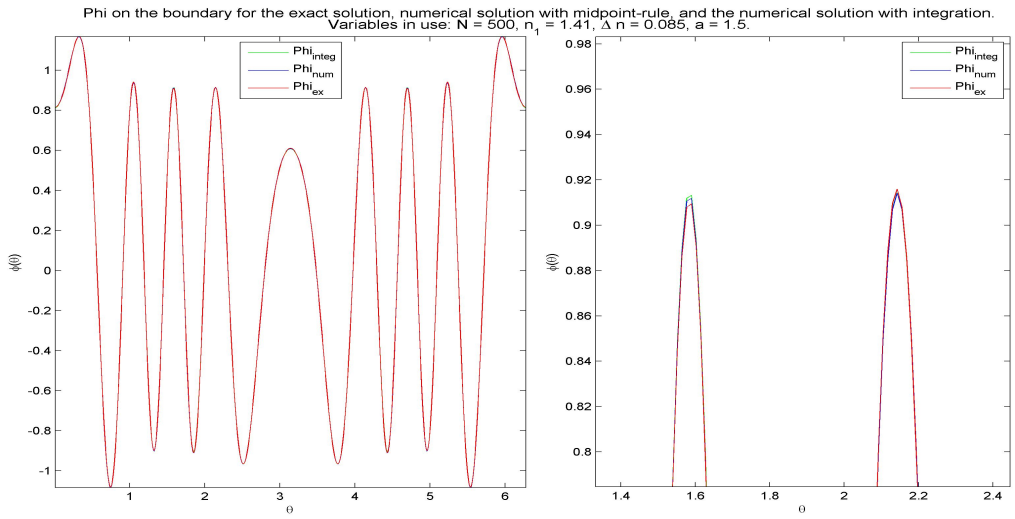

Figure 30: The solution on the boundary of the cylinder is, for most refraction indices, found to be quite good as this plot shows. But it was seen in Figure 28 that there are some refraction indices that give quite inaccurate results for the wave function.

the three solutions from each other. Table 1 shows parts of the vector for the wave function found using the three different methods. The result for two different refraction indices, one "good" and one "bad", are given at two different places on the boundary. By looking at the numbers in this table, the solution found using the integration function is clearly a better choice. The value of φ_{integ} is a better solution than φ_{num} for all the real numbers in the table. For the imaginary numbers, it is found that φ_{num} is actually closer to the exact values for the second example of the vector of the wave function for $\Delta n = 0.085$ (the last three rows). But the values for this refraction index is closer to each other than for $\Delta n = 0.0715$, hence using the integration method has a bigger value for the two areas on the refraction index interval that have been mentioned.

Table 1: The table gives some example values of the wave function on the boundary of the cylinder for the exact solution, the numerical solution, and the solution found using the integration function *quadl* from *Matlab*. Examples are given for two different refraction indices, and for two different areas on the cylinder.

$\Delta n = 0.0715$	*The value of* φ *on the boundary, for* $\theta \in [1.732, 1.771]$ *(800 grid points)*					
φ_{ex}	-0.1942-0.8742i	-0.2770-0.8524i	-0.3573-0.8230i	-0.4345-0.7864i	-0.5078-0.7430i	-0.5766-0.6931i
φ_{integ}	-0.1909-0.8456i	-0.2738-0.8224i	-0.3541-0.7916i	-0.4311-7536i	-0.5043-0.7087i	-0.5728-0.6574i
φ_{num}	-0.2340-0.9282i	-0.3169-0.9050i	-0.3973-0.8742i	-0.4744-0.8362i	-0.5476-0.7914i	-0.6163-0.7401i
$\Delta n = 0.0715$	*The value of* φ *on the boundary, for* $\theta \in [2.242, 2.282]$ *(800 grid points)*					
φ_{ex}	0.4626-0.8266i	0.4019-0.8600i	0.3394-0.8885i	0.2755-0.9123i	0.2105-0.9312i	0.1448-0.9452i
φ_{integ}	0.4724-0.7862i	0.4118-0.8203i	0.3494-0.8497i	0.2855-0.8745i	0.2204-0.8945i	0.1545-0.9097i
φ_{num}	0.4319-0.8678i	0.3714-0.9019i	0.3090-0.9313i	0.2451-0.9560i	0.1801-0.9760i	0.1143-0.9912i
$\Delta n = 0.085$	*The value of* φ *on the boundary, for* $\theta \in [1.732, 1.771]$ *(800 grid points)*					
φ_{ex}	-0.1615-0.8617i	-0.2433-0.8432i	-0.3229-0.8174i	-0.3997-0.7844i	-0.4729-0.7447i	-0.5421-0.6986i
φ_{integ}	-0.1641-0.8623i	-0.2460-0.8427i	-0.3256-0.8156i	-0.4023-0.7814i	-0.4754-0.7404i	-0.5444-0.6930i
φ_{num}	-0.1663-0.8726i	-0.2483-0.8529i	-0.3280-0.8258i	-0.4047-0.7916i	-0.4779-0.7507i	-0.5470-0.7033i
$\Delta n = 0.085$	*The value of* φ *on the boundary, for* $\theta \in [2.242, 2.282]$ *(800 grid points)*					
φ_{ex}	0.5148-0.7804i	0.4580-0.8179i	0.3992-0.8510i	0.3385-0.8795i	0.2765-0.9034i	0.2134-0.9227i
φ_{integ}	0.5174-0.7720i	0.4608-0.8102i	0.4019-0.8441i	0.3413-0.8735i	0.2792-0.8984i	0.2160-0.9187i
φ_{num}	0.5185-0.7763i	0.4619-0.8144i	0.4031-0.8482i	0.3425-0.8775i	0.2804-0.9023i	0.2173-0.9225i

10 Conclusion

This chapter concludes the thesis by describing the achievements and outlining directions for future work.

10.1 Achievements

The goal for this thesis was to calculate forces and light scattering on two dielectric, infinitely long cylinders placed in a host medium, in order to find bistability. The background for the problem is an experiment on optical binding of two dielectric spheres performed by Metzger et al. [9]. In the experiment bistability and hysteresis in the equilibrium separations of the optically bound dielectric spheres were observed in one dimension.

The setup that has been used in this paper is a simplified version of the setup from the experiment. In the experiment two light sources were used, while in this paper only one source has been used. The reduction in the number of sources were validated in Chapter 3. In addition the three dimensional spheres that were used in the experiment, has been reduced to a two dimensional problem using infinitely long cylinders in this thesis. The waves were expected to behave somewhat different in two compared to three dimensions, but not necessarily affect the bistability that was found in three dimensions.

A method for calculating the force on the two cylinders has been developed, and the result has been compared with the result from the experiment. In the end no bistability was found in two dimensions. The reason why no bistability was found might be because the wave behave differently in two dimension, or that the numerical approximation was just not good enough. Or it might be that some of the assumptions that were taken in the experiment were not good enough. For instance was backscattering of the waves not taken care of. So maybe the bistability was found by coincidence.

Another observation is that in the experiment the bistability disappeared when the difference in the refraction index between the spheres and the host medium got large enough. Increasing the difference in the refraction index leads to stronger bindings between the spheres, which might be the reason why the bistability disappeared. In two dimensions the bindings were found to be stronger than in three dimensions, and this might be the reason why no bistability is found. It might be possible to find areas with bistability in two dimensions by increasing the refraction index of the host medium, but unfortunately the numerical approximation would not handle smaller values of Δn very well.

Even though no bistability was found for the problem in this paper, another interesting phenomenon was discovered. When plotting the lowest values for the force differences between the two cylinders in a refraction index versus displacement diagram, the result indicated an asymptote near

two of the refraction indices. The same asymptotic behavior was found when looking at the minimum values of the potential for different refraction indices. This was seen in Figures 25 and 27 in the previous chapter. When looking into this phenomenon it was discovered that the calculation of the wave function on the boundary of a cylinder is quite inaccurate for certain values of the refraction indices. The inaccuracy was traced back to a simplified solution of the integral equations for the wave function. A midpoint rule was used instead of performing an integration, and for some reason this method were quite inaccurate for some of the refraction indices, while for other indices it gave results quite near the exact solution.

10.2 Future work

Below some issues that should be developed further are mentioned.

- The integral equations that was solved to find the wave function in this paper was solved using a midpoint rule. That means that the value in the middle of the interval multiplied by the width of the interval is used as an approximation for the integration. This is not a very accurate method. A better method should be developed for solving the integrals in a more accurate, but efficient way. The time it takes to perform numerical calculations will always be an issue.
- Developing a method to solve the system in three dimensions to see if the bistability can be found then.
- The asymptotic behavior that was found around two values of the refraction indices is another interesting issue to investigate further.

References

[1] EA Bahaa and M.C. Teich. *Fundamentals of photonics*. Wiley, 1991.

[2] A. Ashkin and JM Dziedzic. Optical Levitation by Radiation Pressure. *Applied Physics Letters*, 19:283, 2003.

[3] W.J. Glantschnig and S.H. Chen. Light scattering from water droplets in the geometrical optics approximation. *Appl. Opt*, 20(14):2499–2509, 1981.

[4] B.T. Draine. The discrete-dipole approximation and its application to interstellar graphite grains. *Astrophysical Journal*, 333(2):848–872, 1988.

[5] I. Brevik. Experiments in phenomenological electrodynamics and the electromagnetic energy-momentum tensor. *Physics Reports*, 52(3):133–201, 1979.

[6] J. Wiersig. Boundary element method for resonances in dielectric microcavities. *Journal of Optics A: Pure and Applied Optics*, 5(1):53–60, 2003.

[7] PA Knipp and TL Reinecke. Boundary-element method for the calculation of electronic states in semiconductor nanostructures. *Physical Review B*, 54(3):1880–1891, 1996.

[8] I. Kosztin and K. Schulten. Boundary Integral Method for Stationary States of Two-Dimensional Quantum Systems. *Arxiv preprint physics/9702022*, 1997.

[9] NK Metzger, K. Dholakia, and EM Wright. Observation of Bistability and Hysteresis in Optical Binding of Two Dielectric Spheres. *Physical Review Letters*, 96(6):68102, 2006.

[10] D. McGloin, AE Carruthers, K. Dholakia, and EM Wright. Optically bound microscopic particles in one dimension. *Physical Review E*, 69(2):21403, 2004.

[11] J.D. Jackson. *Classical Electrodynamics*. John Wiley & Sons, New York, 1999, 3rd ed.

[12] David J.(David Jeffrey) Griffiths. *Introduction to electrodynamics*. Prentice Hall, 1999.

[13] R.K. Bock and A. Vasilescu. *The Particle Detector Briefbook*. Springer, 1998.

[14] E. Kreyszig. *Advanced engineering mathematics*. Wiley New York, 1993.

[15] A. Sommerfeld. *Partial differential equations in physics*. Academic Press New York, 1949.

[16] M. Abramowitz and I.A. Stegun. *Handbook of Mathematical Functions*. Dover Publications, 1965.

[17] Eric W. Weisstein. Trigonometric Addition Formulas. From MathWorld – A Wolfram Web Resource. http://mathworld.wolfram.com/TrigonometricAdditionFormulas.html.

[18] Eric W. Weisstein. Bessel Function of the First Kind. From MathWorld – A Wolfram Web Resource. http://mathworld.wolfram.com/BesselFunctionoftheFirstKind.html, 2004.

[19] S.J. Colley. *Vector calculus*. Prentice Hall Upper Saddle River, NJ, 1998.

[20] R.M.M. Mattheij, SW Rienstra, and JHM ten Thije Boonkkamp. *Partial Differential Equations: Modeling, Analysis, Computation*. Society for Industrial Mathematics, 2005.

[21] I.S. Gradshtejn, I.M. Ryzhik, A. Jeffrey, and D. Zwillinger. *Table of Integrals, Series, and Products*. Elsevier, 2007, 7th ed.

[22] Eric W. Weisstein. Modified Bessel Function of the Second Kind. 2002.

[23] Matlab help files. www.mathworks.com, 2007.

[24] R. Paschotta. Gaussian beams. From Encyclopedia of Laser Physics and Thechnology. http://www.rp-photonics.com/gaussian_beams.html.

[25] Bob Mellish. Diagram of Gaussian beam parameters. English Wikipedia, http://en.wikipedia.org/wiki/Image:Gaussianbeam.png, 2004.

[26] Z. Wu and L. Guo. Electromagnetic scattering from a multilayered cylinder arbitrarily located in a Gaussian beam, a new recursive algorithm. *Prog. Electromagn. Res*, 18:317–333, 1998.

[27] E. Lalor. Conditions for the validity of the angular spectrum of plane waves. *J. Opt. Soc. Am*, 58(9):1235–1237, 1968.

[28] M. Born and E. Wolf. *Principles of Optics: Electromagnetic Theory of Propagation, Interference and Diffraction of Light*. Cambridge University Press, 2000.

[29] VV Kotlyar and AG Nalimov. Calculating the pressure force of the non-paraxial cylindrical Gaussian beam exerted upon a homogeneous circular-shaped cylinder. *Journal of Modern Optics*, 53(13):1829–1844, 2006.

[30] V. Karásek, K. Dholakia, and P. Zemánek. Analysis of optical binding in one dimension. *Applied Physics B: Lasers and Optics*, 84(1):149–156, 2006.